**Scholars Journal of Physics, Mathematics and Statistics**

OPEN ACCESS

Abbreviated Key Title: Sch J Phys Math Stat
ISSN 2393-8056 (Print) | ISSN 2393-8064 (Online)
Journal homepage: https://saspublishers.com

# Light–Matter Strategies for Next-Generation Solar Cells: Active-Medium Architectures, Ultrafast Carrier Dynamics, and Laser-Enabled Photonic Structuring

Esha Eman Aslam[1], Waheed Zaman Khan[2,3*], Mohammed Ateeq Mudassar[2], Usama Yousaf[4], Akhtar Hussain[2], Saqlain Aslam[1], Tariq Majeed[5]

[1]Department of Physics, Government College University Faisalabad, Faisalabad, Punjab 38000, Pakistan
[2]Department of Physics, Division of Science and Technology, University of Education, Lahore, Punjab 54770, Pakistan
[3]Phystech School of Aerospace Technology, Moscow Institute of Physics and Technology (MIPT), Dolgoprudny, Moscow Region 141700, Russian Federation
[4]Institute of Physics, Bahauddin Zakariya University, Multan, Pakistan
[5]Department of Physics, Quaid-i-Azam University, Islamabad, Pakistan

**DOI:** https://doi.org/10.36347/sjpms.2025.v12i10.001 | **Received:** 14.10.2025 | **Accepted:** 22.12.2025 | **Published:** 27.12.2025

***Corresponding author:** Waheed Zaman Khan
Department of Physics, Division of Science and Technology, University of Education, Lahore, Punjab 54770, Pakistan

**Abstract** **Original Research Article**

This review reframes photovoltaic (PV) devices through a light–matter engineering lens, treating the absorber stack as an active medium whose optical, electronic, and thermal pathways must be co-optimized for both efficiency and operational reliability. It surveys how mature platforms (Si, CIGS, CdTe, III–V) and emerging absorbers (perovskites, organics, quantum dots, and 2D semiconductors) respond to optical-field design strategies, and why these strategies become more critical in tandem and multifunctional architectures where spectral and electrical matching govern performance. The methodology emphasizes linking ultrafast and spatially resolved spectroscopy (e.g., carrier relaxation, diffusion, and recombination signatures) to device-relevant loss channels, enabling diagnosis of interface- and grain-boundary-limited operation. Building on this foundation, the review compares plasmonic and dielectric nanostructures, metasurfaces, and photonic textures for light trapping while accounting for parasitic absorption and stability tradeoffs. It then consolidates laser-enabled photonic structuring (ns/ps/fs regimes, LIPSS, direct writing, local defect healing and contact formation) as a scalable route to pattern, repair, and tune thin-film PV stacks. Finally, it outlines fabrication and passivation options and discusses how laser steps can be integrated into manufacturing lines with inline metrology and yield control. Overall, the article provides a device-to-process roadmap for designing PV stacks where optical gains translate into durable, manufacturable performance.

**Keywords:** Photovoltaics, Light–Matter Engineering, Active Medium Architecture, Ultrafast Spectroscopy, Nanophotonics/Metasurfaces, Laser Material Processing (LIPSS), Thin-Film Passivation, Perovskite Solar Cells.



## 1. INTRODUCTION

In the last decade, photovoltaics has evolved from a niche option to a major pillar of the global energy system, driven by steady improvements in device physics, materials engineering, and large scale manufacturing (Green *et al*., 2023). Crystalline silicon solar cells at the research level now report efficiencies above about 26 percent, while commercial modules routinely exceed 22 percent, indicating that this technology is operating only a few absolute percentage points below its theoretical radiative limit for a bandgap near 1.12 eV (Green *et al*., 2023; Saive, 2021). At the same time, metal halide perovskite devices have progressed from early prototypes to single junction cells with efficiencies around 26 to 27 percent, and perovskite silicon tandem architectures have surpassed roughly 33 percent, putting them among the most efficient photovoltaic systems ever demonstrated (Duan *et al*., 2023; Huang *et al*., 2025). These achievements make it clear that further advances will depend less on incremental improvements in bulk material quality and more on deliberate control of how light interacts with complex semiconductor stacks in space, time, and energy (Garnett *et al*., 2021; van der Burgt *et al*., 2020).

The classical detailed balance analysis of Shockley and Queisser shows that even an ideal single junction solar cell is fundamentally limited by sub bandgap transmission, incomplete absorption near the band edge, thermalization of photoexcited carriers, and radiative emission at open circuit, which together restrict the maximum efficiency to roughly one third of the incident solar power for an optimally chosen bandgap (Shockley & Queisser, 1961; Zanatta, 2022). Crystalline silicon, with a lower bandgap, has a somewhat reduced but still high radiative limit, and current record cells lie close to this ceiling, confirming that this technology is already exploiting a large fraction of its thermodynamically allowed performance (Green *et al*., 2023; Saive, 2021). When realistic non radiative recombination, series and shunt resistances, and parasitic optical losses in contacts and encapsulation layers are included, the gap between practical devices and their radiative limits can be understood as the sum of many small but coupled loss channels rather than a single dominant deficit (Saive, 2021; Zanatta, 2022). As record efficiencies continue to climb, loss mechanisms that were once considered secondary, such as photon recycling, angular and spectral control of emission, hot carrier cooling rates, and interface specific recombination, become central design targets for the next generation of devices (Garnett *et al*., 2021; van der Burgt *et al*., 2020).

Emerging absorber families introduce additional light matter phenomena that can be either exploited or must be controlled. Metal halide perovskites, organic bulk heterojunctions, colloidal quantum dots, and low dimensional semiconductors exhibit strong excitonic effects, defect tolerance, polaron formation, and in some cases relatively slow hot carrier cooling, making their photophysics highly sensitive to local fields, microstructure, and interface chemistry (Li *et al*., 2020; Qiu *et al*., 2023). Ultrafast spectroscopic studies reveal that carrier cooling, trapping, and interfacial charge transfer in these materials often occur on femtosecond to nanosecond timescales and can be significantly modified by compositional tuning, passivation treatments, and contact engineering (Li *et al*., 2020; Gong *et al*., 2023). As a result, the distribution of the optical field inside the device, including interference patterns, scattering resonances, and guided modes, directly influences not only how many photons are absorbed but also how carriers relax, migrate, and recombine before extraction (Garnett *et al*., 2021; Li *et al*., 2020). This situation makes the electromagnetic environment an active design variable that must be engineered with the same care as band structure and defect landscape (Garnett *et al*., 2021; van der Burgt *et al*., 2020).

These considerations are especially acute in tandem and multi junction architectures, where different subcells share the solar spectrum and must be optically and electrically matched. In perovskite silicon tandems, for example, the thickness and bandgap of the perovskite top cell, the refractive indices of transport and recombination layers, and the morphology of textured interfaces together determine current matching, voltage retention, and parasitic absorption, as well as the strength of local electric fields that drive ion migration and interfacial degradation (Duan *et al*., 2023; Huang *et al*., 2025). Stability studies show that local heating and field distributions created by optical design and encapsulation can accelerate or slow key degradation pathways, so photon management strategies cannot be evaluated purely on the basis of initial efficiency (Baumann *et al*., 2023; Duan *et al*., 2023). Similar couplings arise in organic and quantum dot devices, where nanostructuring intended for light trapping also alters morphology, phase segregation, and interfacial energetics, with direct consequences for recombination dynamics and long term reliability (Li *et al*., 2020; Qiu *et al*., 2023).

At the same time, advanced light matter concepts must remain compatible with industrial constraints. Long term deployment requires that devices withstand decades of illumination, temperature cycling, humidity, and mechanical stress while maintaining acceptable power output, especially for emerging materials that are more chemically and mechanically fragile than crystalline silicon (Baumann *et al*., 2023). Techno economic analyses indicate that decisions about optical design, interconnection schemes, and laser processing steps strongly influence levelized cost of electricity once technologies move from champion cells to large scale module production, because they affect material consumption, process complexity, yield, and repair strategies (Cordell *et al*., 2023). In this context, photonic and laser based structuring need to be assessed not only for their impact on current, voltage, and fill factor but also for their effects on processing windows, encapsulation strategies, and integration into existing production lines (Jamaatisomarin *et al*., 2023; Palma, 2020).

Taken together, these developments motivate a light matter framework for next generation solar cells that is built on three tightly connected pillars. The first pillar is the concept of active medium architectures, which encompasses the absorber and all adjacent functional layers that participate in light absorption, charge generation, transport, and recombination, and which determines the spatial distribution of both the optical field and electronic potentials (Green *et al*., 2023; Duan *et al*., 2023). The second pillar is ultrafast carrier dynamics, probed by techniques such as transient absorption, time resolved photoluminescence, and time resolved terahertz conductivity, which reveal how photoexcited carriers evolve on femtosecond to microsecond timescales and which microscopic processes limit quasi Fermi level splitting and current extraction (Li *et al*., 2020; Gong *et al*., 2023; Qiu *et al*., 2023). The third pillar is laser enabled photonic structuring, including nanophotonic textures,

metasurfaces, and laser processed features that tailor reflection, absorption, emission, and local morphology and that can be implemented in scalable manufacturing flows (Garnett *et al*., 2021; Jamaatisomarin *et al*., 2023; Palma, 2020). In this review, light matter strategies refer to deliberate combinations of these three pillars designed to push photovoltaic devices closer to their thermodynamic limits while simultaneously satisfying the demands of stability, scalability, and techno economic viability (Garnett *et al*., 2021; Baumann *et al*., 2023; Cordell *et al*., 2023).

## 2. Active-Medium Architectures for Advanced Photovoltaics

### 2.1 Conventional Platforms Revisited: Si, CIGS, CdTe and III-V in the Light-Matter Engineering Era

Crystalline silicon remains the workhorse of the photovoltaic industry and a prime example of how active-medium design has evolved over decades. Modern high-efficiency cells use passivated emitter and rear structures, tunnel-oxide-passivated contacts (TOPCon) or silicon heterojunction architectures in which ultra-thin dielectrics and doped polysilicon or amorphous silicon layers simultaneously passivate the surface and provide carrier-selective contacts (Allen *et al*., 2019; Yu *et al*., 2018). Textured front surfaces, often random pyramids on (100) wafers, in combination with antireflection coatings, reduce front reflection and couple incoming light into oblique paths through the wafer, while rear reflectors and locally opened metal contacts enhance internal reflection without excessive recombination (Saive, 2021; Um *et al*., 2021). At the module level, as sketched on the right-hand side of Figure 2.1, the cell stack is laminated between glass and polymer encapsulants with backsheet foils and busbars, turning the entire assembly into an extended optical and thermal environment that governs angular response, operating temperature, and mechanical reliability under field conditions (Green *et al*., 2023).

Even in this mature platform, light-matter limits and thermal constraints are still being actively engineered. Detailed loss analyses show that residual front reflection, parasitic absorption in antireflection coatings and metallization, as well as incomplete luminescence extraction and free-carrier absorption in heavily doped regions, still cost several tenths of a percentage point each in absolute efficiency (Saive, 2021; Green *et al*., 2023). Under high irradiance or in concentrator operation, local heating around metallized regions and at cell interconnects leads to additional thermalization losses and accelerated degradation, which has motivated new encapsulant formulations and backsheet designs with improved thermal conductivity and reflectance (Pakhanov *et al*., 2018). Crystalline silicon therefore illustrates that, even when bulk lifetimes and surface passivation are close to optimized, there is still meaningful room for improvement by tuning the active medium as a coupled optical-electronic-thermal system.

CIGS thin-film technology, represented on the left-hand side of Figure 1, offers a contrasting example where a very thin, strongly absorbing semiconductor must be supported by carefully engineered window, buffer and back-contact layers. A typical high-efficiency CIGS stack consists of a glass substrate, a molybdenum back contact that also acts as a partial reflector, a 1.5-3 μm Cu(In,Ga)Se2 absorber with bandgap grading through the Ga profile, a CdS buffer and a ZnO/ZnO:Al bilayer as transparent conductor (Elhady *et al*., 2021; Kovacic *et al*., 2019). The high absorption coefficient of CIGS allows such thin layers to absorb most of the above-bandgap light, but only if parasitic absorption in the CdS window and TCO is minimized and if back reflection is strong over the relevant spectral range (Oliveira *et al*., 2022; Manzoor *et al*., 2017). Light-management studies have shown that textured back reflectors, diffractive patterns and high-index interlayers at the rear interface can significantly enhance path length and current in ultra-thin CIGS, especially when absorber thickness is pushed below 1 μm for material savings and mechanical flexibility (Kovacic *et al*., 2019; Oliveira *et al*., 2022).

From the active-medium viewpoint, CIGS also demonstrates how composition and microstructure couple to optical design. Bandgap grading, achieved by varying the Ga/(In+Ga) ratio, not only optimizes current-voltage tradeoffs but also shapes the internal electric field and reduces back-surface recombination, which interacts with rear mirror design to determine where photogenerated carriers are collected or lost (Elhady *et al*., 2021; Oliveira *et al*., 2022). Grain boundaries and secondary phases, which are inherent to polycrystalline growth, introduce local variations in refractive index and defect density, so passivation and alkali treatments (for example Na and K incorporation) play dual roles in improving both electronic and optical homogeneity (Elhady *et al*., 2021). As efficiencies approach 23 percent at the cell level, remaining losses in CIGS are increasingly attributed to parasitic absorption in window/buffer layers, incomplete rear reflection, and thermalization in high-energy parts of the spectrum, all of which are targets for more refined light-matter engineering (Oliveira *et al*., 2022; Light Management Tutorial, 2024).

CdTe thin-film modules share many structural similarities with CIGS but have their own characteristic active-medium challenges. Standard designs employ a glass/transparent-conductor/CdS/CdTe/back-contact stack, often with SnO2:F or Cd2SnO4 as the front transparent conductor and a thin CdS window to balance optical losses with junction quality (Romeo *et al*., 2021; Ahmad *et al*., 2023). As in CIGS, the CdTe absorber can be only 3-8 μm thick due to its large absorption coefficient, so textures on the superstrate glass, intentional roughness at the TCO interface, and reflective back contacts are used to scatter light and extend optical path length (Oliveira *et al*., 2022; Hall *et al*., 2021).

Recent efficiency gains to above 22 percent have come from a combination of better front-window design, more transparent and conductive TCOs, CdS thinning, and back-contact optimization, including the use of copper-containing layers and advanced buffer materials that provide good band alignment while maintaining low recombination rates (Romeo *et al*., 2021; Hall *et al*., 2021).

In CdTe, the back contact is a particularly clear example of an active-medium bottleneck. The large valence band offset between CdTe and many metals makes it difficult to form low-resistance ohmic contacts without inducing recombination-active defects or copper-driven instability (Hall *et al*., 2021; Romeo *et al*., 2021). Back-contact engineering therefore simultaneously targets band alignment, defect passivation, optical reflectance and chemical robustness, often through multi-layer stacks that combine a p+-type back surface region, a high-work-function interlayer and a metallic reflector. This multi-functional design directly affects how long-wavelength photons are recycled between front and rear interfaces and how efficiently minority carriers are collected, linking optical management to long-term stability and module lifetime (Hall *et al*., 2021; Ahmad *et al*., 2023).

III-V technologies, widely used in space and concentrator photovoltaics, push the idea of active-medium design to its logical extreme through monolithic multijunction stacks that are finely tuned in bandgap, thickness and refractive index. State-of-the-art devices combine InGaP, GaAs, InGaAs and Ge subcells grown epitaxially on a single substrate with tunnel junctions in between, and employ carefully designed double antireflection coatings and back reflectors to manage light across a broad spectral range under high concentration (Li *et al*., 2021; Yamaguchi *et al*., 2021; Baiju *et al*., 2022). Because each subcell absorbs a specific part of the spectrum, the thickness and optical constants of every layer in the stack must be co-optimized so that current matching is achieved while minimizing parasitic absorption and reflection at internal interfaces (Li *et al*., 2021; Raisa *et al*., 2025). High external luminescence efficiency and photon recycling are critical for approaching the detailed-balance limits in these devices, so emission control and refractive-index engineering are core elements of their active-medium design (Yamaguchi *et al*., 2021).

Despite their high efficiencies, III-V cells face practical limitations in terms of material cost, lattice-mismatch strain, thermal management under concentration and mechanical robustness in space environments. These constraints have motivated extensive work on lightweight III-V-on-foil concepts, inverted metamorphic stacks and advanced thermal spreading layers that can dissipate heat while preserving optical performance (Baiju *et al*., 2022; Yamaguchi *et al*., 2021). As in the thin-film technologies, textured or patterned interfaces, distributed Bragg reflectors and wavelength-selective filters are increasingly used to fine-tune both absorption and emission, showing that even in these premium devices, light-matter strategies are central to both performance and reliability.

Taken together, crystalline silicon, CIGS, CdTe and III-V technologies demonstrate that "conventional" platforms already embed sophisticated active-medium architectures where passivated contacts, graded compositions, textured interfaces and back reflectors have been refined over decades. Figure 2.1 distills some of these ideas by contrasting wafer-based and thin-film modules in terms of stack structure, absorber thickness and interconnection schemes. Revisiting these technologies through a light-matter lens highlights both the robustness of existing design rules and the remaining optical, electronic and thermal losses that motivate the more aggressive nanophotonic, ultrafast-dynamics and laser-structuring strategies discussed in later sections.

Here you re-examine mature technologies such as crystalline silicon, CIGS, CdTe and III–V cells as benchmarks for light–matter engineered design. The subsection can discuss how passivated contacts, back reflectors, textured interfaces and graded compositions already implement hidden “active-medium” strategies. You then identify where optical, electronic and thermal limits still remain, motivating why even these classic platforms benefit from more deliberate light–matter control. This also provides a reference point for comparing emerging materials.

### 2.2 Emerging Absorbers: Perovskites, Organics, Quantum Dots, and 2D Semiconductors

Metal halide perovskites have rapidly transformed from a laboratory curiosity into a leading class of emerging absorbers because they combine solution processability, strong optical absorption, long carrier diffusion lengths, and an unusual degree of defect tolerance compared with conventional semiconductors (Ma *et al*., 2023; Basumatary, 2022). Defect tolerance arises from a band structure in which many common point defects create shallow states near band edges rather than deep traps, so moderate defect densities do not immediately quench open-circuit voltage or fill factor (Basumatary, 2022; Abbas *et al*., 2024). Recent work has extended this concept to “dynamic” defect tolerance, showing that in halide perovskite nanocrystals and thin films, fluctuating defect configurations and polaronic screening allow even hot carriers to remain relatively insensitive to certain trap populations on ultrafast time scales (Ye *et al*., 2024; Mosquera-Lois *et al*., 2025). Bandgap engineering through cation alloying, halide mixing, dimensional reduction, and even pressure tuning enables perovskites to cover a wide spectral range from the near ultraviolet to the near infrared, which is central for both single-junction optimization and tandem design (Miah *et al*., 2024; Ma *et al*., 2023).

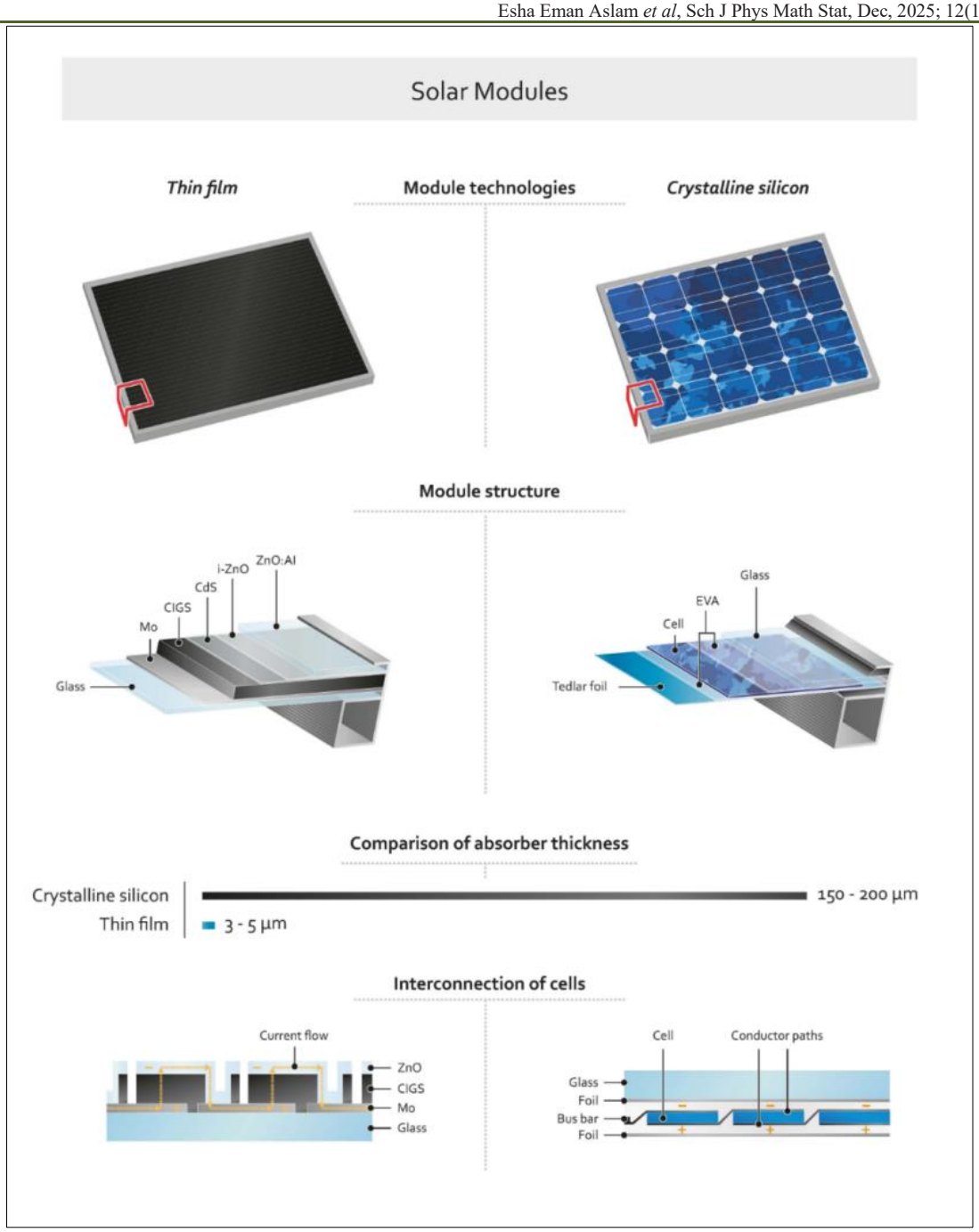


**Figure 1: Conventional thin-film and crystalline silicon module architectures as active media**

Ultrafast spectroscopic studies reveal that photoexcited carriers in perovskites typically thermalize within hundreds of femtoseconds to a few picoseconds, but retain long diffusion lengths due to low trap-assisted recombination and relatively benign grain boundaries (Li *et al*., 2020; Ma *et al*., 2023). These dynamics are highly sensitive to composition, microstructure, and interfacial energetics, so transport layers and passivation schemes must be co-engineered with the absorber to preserve quasi-Fermi level splitting and minimize nonradiative losses (Abbas *et al*., 2024; Chen *et al*., 2024). At the same time, the soft ionic lattice and mixed ionic–electronic conduction introduce vulnerabilities, including ion migration under bias or illumination, phase segregation in mixed halide compositions, and interfacial chemical reactions with metal contacts or transport layers that can accelerate degradation (Abbas *et al*., 2024; Ma *et al*., 2023). Compositional and interfacial engineering strategies, such as low dimensional perovskite capping layers, Lewis acid–base surface treatments, and 2D material interlayers, are therefore used as design knobs to stabilize interfaces, suppress deep defects, and control light absorption and emission simultaneously (Miah *et al*., 2024; Miao *et al*., 2022; Imran *et al*., 2025).

Organic solar cells treat the active layer as a molecularly designed bulk-heterojunction of donor and

acceptor species, where strong excitonic effects and nanoscale phase separation are central features rather than complications (Li *et al*., 2022; Solak *et al*., 2023). Excitons must dissociate at donor–acceptor interfaces, so the morphology of interpenetrating domains and the energetic offset between donor and acceptor frontier orbitals control both charge generation efficiency and voltage losses (Scharber & Sariciftci, 2013; Asanov *et al*., 2024). The shift from fullerene to non-fullerene acceptors has enabled much stronger absorption, more favorable energy level alignment, and reduced nonradiative losses, pushing single-junction organic solar cell efficiencies close to or above 19 percent in recent reports (Li *et al*., 2022; Liu *et al*., 2023; Fu *et al*., 2024). Because these materials are intrinsically flexible, mechanically compliant, and amenable to low-temperature coating, they are attractive active media for semi-transparent, flexible, and building-integrated photovoltaics, where optical design and mechanical robustness must be balanced (Solak *et al*., 2023; Zhu *et al*., 2024).

Organic absorbers are, however, sensitive to oxygen, moisture, and photochemical degradation, and they typically exhibit lower dielectric constants than inorganic semiconductors, which increases Coulomb binding and makes exciton dissociation more demanding (Li *et al*., 2022; Asanov *et al*., 2024). This vulnerability is increasingly addressed through molecular design that optimizes backbone rigidity, noncovalent locking, and end-group chemistry, as well as through the introduction of multi-component or ternary blends that can synergistically broaden absorption and enhance morphological stability (Fu *et al*., 2024; Li *et al*., 2022). Interlayers and electrodes are also treated as active parts of the optical and electronic medium, with work-function-tuned contacts, self-assembled monolayers, and 2D materials used to improve band alignment, reduce interfacial recombination, and tailor angular and spectral response (Solak *et al*., 2023; Imran *et al*., 2025).

Colloidal quantum dots (QDs) and perovskite quantum dots represent another powerful class of tunable active media, where quantum confinement enables precise control of bandgap and absorption spectrum by adjusting particle size and composition (Shilpa *et al*., 2023; Lee *et al*., 2024). QD-based solar cells and quantum-dot-sensitized architectures have progressed from sub-percent efficiencies to values exceeding 18 percent in optimized devices, while maintaining the potential for low-temperature, solution-processed fabrication on diverse substrates (Shilpa *et al*., 2023; Kim *et al*., 2019; Jang *et al*., 2024). Core–shell structures, ligand exchange, and surface passivation are key levers to suppress nonradiative surface recombination and improve carrier transport between dots, effectively transforming a collection of nanocrystals into a coherent electronic and optical medium (Lee *et al*., 2024; Kumar *et al*., 2023). QDs can also be integrated as intermediate bands, spectral converters, or energy-transfer layers in multi-junction and hybrid devices, where their tunable absorption and strong interaction with local fields are exploited for light management and hot-carrier harvesting concepts (Shilpa *et al*., 2023; Albaladejo-Siguan *et al*., 2021; Kim *et al*., 2019).

Stability remains a central challenge for QD-based devices, since surface ligands, interfaces, and grain boundaries are highly reactive under illumination, heat, and electric fields, leading to trap formation and performance loss over time (Albaladejo-Siguan *et al*., 2021; Kumar *et al*., 2023). Encapsulation strategies, inorganic ligand shells, and hybrid architectures in which QDs are embedded within more robust matrices are being developed to mitigate these issues while preserving bandgap tunability and processability (Lee *et al*., 2024; Shilpa *et al*., 2023). In parallel, ultrafast spectroscopy is being used to map energy-transfer pathways, carrier cooling, and multi-exciton generation in QD films, providing guidance for designing QD-based active media that best exploit light–matter interactions in the visible and infrared (Lee *et al*., 2024; Shilpa *et al*., 2023).

Two-dimensional semiconductors and related layered materials add yet another dimension of tunability, since their electronic structure, exciton binding energies, and optical response are strongly thickness-dependent and can be manipulated by stacking, twisting, or forming van der Waals heterostructures (Wang *et al*., 2024; Imran *et al*., 2025). In photovoltaic applications, 2D materials can act as ultrathin absorbers, carrier-selective contacts, passivation layers, or charge-transport interlayers, with reported devices ranging from 2D–2D homojunctions and p–n junctions to 2D–3D heterostructures that combine layered materials with silicon or perovskites (Cho *et al*., 2018; Miao *et al*., 2022; Ding *et al*., 2025). For example, $MoS_2$, $WS_2$, and related transition-metal dichalcogenides can be used to passivate perovskite surfaces, enhance crystallization, and improve band alignment, leading to gains in both efficiency and operational stability (Miao *et al*., 2022; Ali Ahmad *et al*., 2021; Imran *et al*., 2025).

2D materials also introduce new routes for light–matter engineering, because their high refractive indices, anisotropic optical response, and strong excitonic resonances enable integration into photonic cavities, metasurfaces, and waveguides at nanometer thicknesses (Wang *et al*., 2024; Gatade *et al*., 2024). However, environmental sensitivity, interfacial contamination, and contact resistance remain persistent issues, so encapsulation, surface cleaning, and contact engineering must be tailored with the same care as band-structure design (Imran *et al*., 2025; Wang *et al*., 2024). When combined with perovskites, organics, or QDs in hybrid stacks, 2D materials can thus be viewed as multifunctional components that modulate absorption,

passivate defects, and tune carrier extraction, fully in line with the active-medium concept that underpins this review (Miao *et al*., 2022; Imran *et al*., 2025).

### 2.3 Device-Level Architectures: Single-Junction, Tandem, and Multi-Functional Stack Designs

Single-junction architectures remain the foundational configuration for both conventional and emerging photovoltaic technologies, and they are typically optimized around a single absorber whose bandgap and thickness are chosen to balance current and voltage under a standard solar spectrum (Ma *et al*., 2023; Li *et al*., 2022). In crystalline silicon and perovskite single-junction devices, continued gains have come from integrating passivating contacts, optimizing front and rear textures, and carefully managing parasitic absorption in transport and encapsulation layers so that the active medium operates close to its radiative limit (Ma *et al*., 2023; Abbas *et al*., 2024). For emerging absorbers such as organics, QDs, and 2D materials, single-junction layouts provide clean testbeds for understanding how exciton diffusion, interfacial dissociation, and thickness-dependent absorption constrain device performance and how optical design can compensate for limited diffusion lengths or suboptimal mobilities (Li *et al*., 2022; Shilpa *et al*., 2023; Wang *et al*., 2024).

As laboratory efficiencies of single-junction perovskites approach and surpass 26 percent and organic devices exceed 19 percent, the motivation for tandem and multi junction architectures becomes increasingly strong, because these configurations can reduce thermalization and transmission losses by splitting the spectrum between absorbers of different bandgaps (Ma *et al*., 2023; Liu *et al*., 2023; Jamesh *et al*., 2025). Perovskite–silicon tandems are the most developed example, with reported power-conversion efficiencies above 32 percent and projections that practical modules could significantly beat the single-junction silicon limit once stability and manufacturing are matured (Huang *et al*., 2025; Jamesh *et al*., 2025). In these architectures, the perovskite top cell is typically tuned to a bandgap of 1.7–1.8 eV, while the silicon bottom cell retains its 1.1 eV bandgap, and the combined optical and electrical design must ensure current matching, minimal optical losses at interfaces, and effective recombination in the interconnection region (Huang *et al*., 2025; Ma *et al*., 2023).

From a circuit perspective, perovskite-based tandems are usually categorized as two-terminal monolithic, four-terminal mechanically stacked, and three-terminal hybrid configurations, each of which imposes different constraints on the active medium and light-management strategy (Huang *et al*., 2025; Rafiq *et al*., 2024). Two-terminal monolithic tandems connect subcells in series, requiring strict current matching and a well-designed recombination junction that simultaneously serves as an optical spacer, electrical interconnect, and often a diffusion barrier (Ma *et al*., 2023; Suman *et al*., 2025). Four-terminal tandems, by contrast, allow each subcell to operate at its own maximum power point and relax current-matching requirements, but they introduce additional optical interfaces, packaging complexity, and cost (Rafiq *et al*., 2024; Cordell *et al*., 2025). Three-terminal designs represent an intermediate approach in which some degree of independent current extraction is possible while preserving a compact stack, and they are particularly interesting when one of the subcells is based on an emerging absorber such as an organic or QD layer (Huang *et al*., 2025; Rafiq *et al*., 2025).

Tandem devices are not limited to perovskite–silicon combinations; perovskite–perovskite, perovskite–CIGS, perovskite–organic, and perovskite–TMDC tandems have all been proposed and experimentally demonstrated in various forms (Rafiq *et al*., 2024; Suman *et al*., 2025; Shilpa *et al*., 2023). In many of these stacks, the top absorber is a wide-bandgap perovskite or organic material that captures high-energy photons, while the bottom cell is based on a narrower-bandgap inorganic or QD absorber that harvests longer wavelengths, so light-management and spectral splitting become explicit design variables of the active medium (Jamesh *et al*., 2025; Li *et al*., 2022). The introduction of 2D materials as transport layers, passivation interlayers, or even active subcells in such tandems adds further tunability, because their thickness, work function, and optical constants can be adjusted to optimize both electronic selectivity and optical interference (Imran *et al*., 2025; Miao *et al*., 2022; Wang *et al*., 2024).

Multi-functional stack designs push the active-medium concept further by demanding that individual layers simultaneously perform optical, electronic, mechanical, and stability roles. For instance, in many perovskite–silicon tandems the recombination junction and adjacent transport layers are designed to act as optical spacers that enhance constructive interference in the perovskite top cell, as electrical recombination regions with minimal voltage loss, and as chemical barriers that block ion migration and interdiffusion between subcells (Huang *et al*., 2025; Abbas *et al*., 2024). Similarly, organic and QD interlayers can be engineered to both passivate defects and serve as spectral converters or luminescent coupling layers that recycle sub-bandgap or off-angle photons back into the active regions, improving current and open-circuit voltage in complex stacks (Lee *et al*., 2024; Shilpa *et al*., 2023). MXene and other 2D materials provide examples where a single nanometer-thick layer can increase conductivity, tune contact work function, enhance optical absorption via plasmonic or interference effects, and improve environmental stability when used as a barrier or encapsulation layer (Pandey *et al*., 2025; Imran *et al*., 2025).

In all these architectures, the interplay between optical design, ultrafast carrier dynamics, and long-term reliability is increasingly being evaluated through combined experimental and techno-economic analyses. For example, cost models for perovskite–silicon tandems show that the choice of stack architecture, subcell integration strategy, and laser or patterning steps for interconnection can have impacts on levelized cost of electricity that are comparable in magnitude to the raw efficiency gains (Cordell *et al*., 2025; Huang *et al*., 2025). At the same time, stability studies reveal that certain design decisions that are favorable for light trapping or current matching, such as strong field concentrations at textured interfaces or high operating voltages in wide-bandgap top cells, can accelerate degradation unless carefully managed by passivation and thermal design (Abbas *et al*., 2024; Jamesh *et al*., 2025; Albaladejo-Siguan *et al*., 2021). Consequently, next-generation device architectures are increasingly planned as multi-functional active media in which light–matter interaction, carrier dynamics, and durability are co-optimized rather than treated as separate stages in the design process (Ma *et al*., 2023; Imran *et al*., 2025).

## 3. Semiconductor Materials and Interface Physics under Optical Excitation

### 3.1 Band Alignment, Built-In Fields, and Charge-Selective Contacts

According to Figure 2, modern crystalline-silicon solar cells rely on carefully engineered band alignment and built-in fields at the contacts to turn a bare c-Si wafer into a carrier-selective photovoltaic stack. In a simple TCO/c-Si junction, the band bending at the interface is set mainly by the wafer doping and the TCO work function, so both electrons and holes can reach the contact and recombine, which limits the open-circuit voltage. By contrast, silicon heterojunction (SHJ) and passivating-contact devices introduce thin passivating layers and carrier-selective contact stacks that reshape the conduction and valence bands so that electrons and holes follow different preferred pathways out of the device (Allen *et al*., 2019; Lin *et al*., 2023).

In the classical SHJ architecture sketched in Figure 2(a–b), intrinsic hydrogenated amorphous silicon (a-Si:H(i)) is first deposited on the textured c-Si surface to chemically passivate dangling bonds and reduce interface defect density. On top of this, p-type and n-type a-Si:H layers are added as hole- and electron-selective contacts. Their wider bandgap and suitable electron affinity create valence- and conduction-band offsets that bend the c-Si bands near each interface. At the hole contact, the valence band aligns so that holes see only a small barrier while electrons face a large barrier; at the electron contact, the situation is reversed. Under illumination, these built-in fields steer photogenerated holes and electrons toward their respective contacts while maintaining a large quasi-Fermi level splitting in the c-Si bulk (Allen *et al*., 2019; Zhou *et al*., 2022).

Figure 2(d–f) then illustrates how poly-Si/$SiO_x$ passivating contacts (often referred to as TOPCon-type structures) refine this idea. Here, an ultrathin $SiO_x$ tunnel oxide provides excellent chemical and field-effect passivation, and a heavily doped $n^+$ or $p^+$ poly-Si layer on top fixes the contact work function and drives strong band bending in the underlying c-Si. Majority carriers tunnel through the thin oxide with low resistance, whereas minority carriers are blocked by the barrier and repelled by the electric field. When the $SiO_x$ thickness, poly-Si doping and hydrogenation are optimized, these contacts reach extremely low recombination currents while keeping contact resistivity in the milliohm-centimeter-squared range, enabling cell efficiencies above about 24–26% in industrial SHJ and TOPCon devices (Lin *et al*., 2023; Wei *et al*., 2023; Yan *et al*., 2021; Zhou *et al*., 2022).

The lower panels of Figure 2 also highlight dopant-free asymmetric heterocontact concepts, where thin wide-bandgap metal oxides or fluorides replace doped silicon as the selective contact layer. Electron-selective oxides such as $TiO_x$ or $Ta_2O_5$ are chosen so that their conduction band lies close to that of c-Si while their valence band sits far below, giving a small barrier for electrons but a large barrier for holes. Conversely, high-work-function oxides such as $MoO_x$ align favorably with the valence band of c-Si and strongly block electrons, so they act as hole-selective contacts (Wang *et al*., 2023; Zeng *et al*., 2022). Work from the Javey research lab has shown that, when combined with a thin intrinsic passivation layer, such dopant-free electron and hole contacts can support high open-circuit voltages and low series resistance without any high-temperature diffusion steps, yielding efficient “DASH” (dopant-free asymmetric heterocontact) silicon solar cells (Bullock *et al*., 2016, 2018; Allen *et al*., 2019).

Overall, Figure 2 makes clear that band alignment and built-in fields are practical design knobs rather than fixed material properties. Intrinsic or wide-bandgap layers are used to decouple surface passivation from carrier selectivity, while the choice of doped or dopant-free contact materials, their work functions, and any interfacial dipoles are tuned so that c-Si experiences strong, well-oriented internal fields and each terminal behaves as an almost ideal electron or hole filter. Under optical excitation, this engineered energy-band landscape allows the device to harvest most of the internal quasi-Fermi level splitting with minimal contact recombination—providing a concrete silicon benchmark for the broader discussion of carrier-selective interfaces in other semiconductor and perovskite systems.

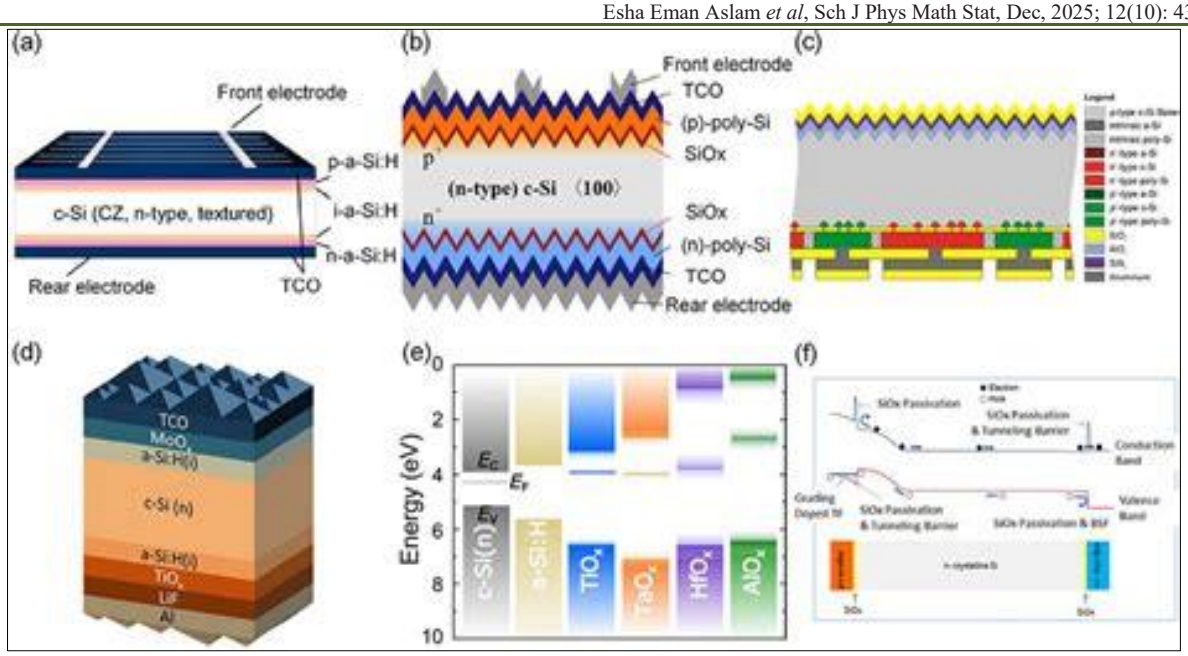


**Figure 2: Energy-Band Landscape and Built-In Fields in a Silicon Heterojunction with Carrier-Selective Contacts**

Cross-sections of crystalline-silicon heterojunction solar cells using amorphous or poly-Si carrier-selective contacts (top) are shown together with representative energy-band diagrams (bottom). The intrinsic amorphous or tunnel-oxide layers chemically passivate the c-Si surface, while adjacent n- and p-type layers plus transparent conducting oxides create band offsets and strong built-in fields that selectively extract electrons and holes. The comparison between different heterocontact stacks illustrates how work-function engineering, band alignment and layer sequence control the internal electric field and allow efficient harvesting of quasi-Fermi level splitting in modern silicon heterojunction architectures.

### 3.2 Defects, Traps, and Non-Radiative Recombination at Bulk and Interfaces

Under illumination, any departure from an ideal, defect-free lattice opens non-radiative loss channels that shorten carrier lifetimes and limit the achievable quasi-Fermi level splitting. In both crystalline semiconductors and metal–halide perovskites, most of these losses are well described by Shockley–Read–Hall (SRH) statistics, where deep defect levels in the bandgap capture and emit carriers asymmetrically and thus act as efficient recombination centers (Shockley & Read, 1952). When such traps lie near midgap and possess large capture cross-sections, they strongly compete with radiative bimolecular and Auger recombination, especially at the low and moderate carrier densities relevant for photovoltaic operation (Herz, 2016; deQuilettes *et al*., 2019).

In bulk crystalline silicon, typical SRH centers arise from transition-metal impurities (such as Fe, Ni, and Cu) and from point-defect complexes introduced during growth, gettering, or high-temperature processing. Their impact is routinely quantified via effective minority-carrier lifetime measurements and modeled using SRH lifetimes that depend on defect energy levels, capture cross-sections, and defect densities. Related physics applies in metal–halide perovskites, but here the defect chemistry is dominated by halide vacancies, interstitials, antisites, and under-coordinated Pb or Sn sites created by slight deviations from stoichiometry, incomplete crystallization, or ion migration (Herz, 2016; Manser, Christians, & Kamat, 2016). Despite relatively high nominal defect densities, several perovskite compositions exhibit a degree of "defect tolerance," where many traps are shallow or weakly coupled to phonons and therefore have a reduced impact on non-radiative recombination.

Extended defects aggravate non-radiative losses by clustering traps into specific regions. In polycrystalline perovskite and thin-film silicon absorbers, grain boundaries, dislocations, and secondary phases often exhibit higher trap densities than the surrounding grains. Nanoscale photoluminescence mapping directly visualizes highly non-uniform carrier lifetimes, with "bright" grains separated by "dark" recombination-active boundaries that dominate device-scale performance (deQuilettes *et al*., 2015; Doherty *et al*., 2020). These defective regions can also act as fast diffusion pathways for mobile ions, coupling defect chemistry to local electric-field redistribution and hysteresis under bias and illumination (Shi *et al*., 2016; deQuilettes *et al*., 2016).

Interfaces in carrier-selective stacks, such as the amorphous/crystalline silicon heterojunction of Figure 2, introduce their own spectrum of electronic states. At the c-Si/a-Si:H(i) interface, unpassivated dangling bonds act as efficient recombination centers, and their effect is often parameterized via an interface recombination velocity rather than a bulk lifetime. Even when the

crystalline bulk is of very high purity, such interface states can dominate the open-circuit voltage. In perovskite devices, analogous interfacial traps at the perovskite/transport-layer and transport-layer/electrode contacts are now recognized as major loss channels, often associated with under-coordinated ions, interdiffusion, or chemical incompatibility between adjacent layers (Herz, 2016; Stranks *et al*., 2019).

Spatially resolved luminescence tools have become central for diagnosing these losses. Full-device photoluminescence and electroluminescence imaging correlates local emission intensity with implied open-circuit voltage, enabling identification of interface-limited regions and buried defects in both perovskite and silicon heterojunction cells (Hameiri *et al*., 2015; Breitenstein *et al*., 2014). For perovskites, time-resolved photoluminescence and transient absorption spectroscopy are routinely used to disentangle trap-assisted monomolecular recombination from radiative and Auger processes, revealing how post-treatments or interface layers suppress non-radiative channels and push materials closer to the radiative limit (Herz, 2016; Stranks & Snaith, 2015).

In the context of Figure 2, the combined picture is that defects and traps, whether in the bulk or at interfaces, locally reduce the quasi-Fermi level splitting and effectively shrink the built-in potential landscape available to photocarriers. This directly erodes the voltage and fill factor that would otherwise be achievable with ideal carrier-selective contacts. The next subsection therefore turns to how interface engineering through dipoles, 2D layers, and passivating interlayers can mitigate these losses while simultaneously shaping light–matter interactions at the heterointerfaces.

**Table 1: Representative defect classes and mitigation strategies in semiconductor photovoltaic stacks**

| Region in stack (relative to Fig. 2) | Dominant defects / traps | Main non-radiative mechanism | Typical diagnostics | Example mitigation / engineering |
|---|---|---|---|---|
| c-Si bulk (wafer) | Metal impurities, vacancies, interstitial complexes | SRH via deep midgap levels | Quasi-steady-state lifetime, injection-dependent $\tau$ | High-purity growth, gettering, hydrogenation |
| a-Si:H(i) / c-Si interface | Dangling bonds, under-coordinated Si | Surface-limited SRH, high surface recomb. | Lifetime vs. thickness, interface recombination $v_s$ | a-Si:H(i) passivation, optimized H content |
| Perovskite bulk | Halide vacancies/interstitials, Pb/Sn under-coordination | Trap-assisted monomolecular recombination | Time-resolved PL, transient absorption | Stoichiometry control, additives, ligand treatments |
| Grain boundaries / trap clusters | Disordered phases, segregated impurities | Localized SRH at extended defects | Nanoscale PL, PEEM, KPFM | 2D capping layers, grain-boundary passivation |
| Perovskite / ETL interface | Under-coordinated ions, rough morphology, interdiffusion | Interfacial SRH, charge-transfer bottlenecks | PL quenching, impedance spectroscopy, EL imaging | SAM-modified oxides, fullerene interlayers |
| Perovskite / HTL interface | Chemical incompatibility, dopant diffusion | Interface-assisted recombination, ion-assisted | Ultrafast charge-transfer studies, EL efficiency | Dipolar SAMs, graded 2D/3D perovskite, buffer layers |

### 3.3 Interface Engineering for Light–Matter Control: Dipoles, 2D Layers, and Interfacial Passivation

Because interfaces govern both recombination and built-in fields, modern carrier-selective device architectures increasingly treat them as active design elements rather than passive boundaries. The heterojunction in Figure 2 already illustrates this: ultrathin intrinsic a-Si:H layers chemically passivate the c-Si surface, while doped a-Si:H or poly-Si layers act as hole- and electron-selective contacts whose work functions and band offsets are tuned to shape the band bending and internal electric fields. The goal is to create interfaces that are simultaneously electrically benign (low trap density, low recombination), energetically selective (favorable level alignment for one carrier type), and optically transparent to the incoming solar spectrum (Allen *et al*., 2019; Yan *et al*., 2021).

A powerful route to such control is the use of interfacial dipoles formed by self-assembled monolayers (SAMs) or other polar molecular layers. When chemisorbed on metals or metal oxides, SAMs establish a well-defined molecular dipole at the interface, shifting the substrate work function by several hundred millielectronvolts and thereby tuning the barrier height for electrons or holes (Ford *et al*., 2014). In perovskite and organic photovoltaics, phosphonic-acid or carboxylic-acid SAMs on $SnO_2$, $TiO_2$, or ITO are used to raise or lower the contact work function, align transport-layer levels with the perovskite bands, and reduce interfacial recombination (Casalini *et al*., 2017;

Qiao & Zuo, 2018). Recent work shows that such monolayers can simultaneously influence film morphology, suppress interfacial traps, and enhance long-term stability, all while adding negligible parasitic absorption because their thickness is on the molecular scale (Fu *et al*., 2025; Yuan, Zhang, & Yang, 2025).

Two-dimensional layers provide a complementary strategy to control light–matter interaction and recombination. In halide perovskites, quasi-2D Ruddlesden–Popper layers grown on top of a 3D absorber act as wide-bandgap caps that passivate surface defects and create graded band edges, funneling photocarriers into the underlying bulk and increasing photoluminescence quantum yield (Milot *et al*., 2016; Stranks, 2019). In silicon and III–V devices, atomically thin materials such as hexagonal boron nitride, $MoS_2$, or graphene can be inserted as tunneling layers that suppress direct chemical recombination while still allowing efficient carrier tunneling, or as optical spacers that modify the local optical mode structure. By properly choosing thickness, dielectric constant, and band offset, these 2D interlayers allow simultaneous tuning of reflection, absorption, exciton dissociation, and carrier selectivity.

Classical dielectric passivation remains essential, especially in silicon heterojunctions. Atomic-layer-deposited $Al_2O_3$ on c-Si combines low interface-state densities with a high density of negative fixed charges that repel minority carriers from the surface, dramatically reducing SRH recombination (Hoex *et al*., 2008; Schmidt *et al*., 2008). Advanced dielectric stacks such as $PO_x/Al_2O_3$ or $SiO_x$/poly-Si further enhance field-effect and chemical passivation, achieving extremely low effective surface recombination velocities on both p- and n-type substrates (Black *et al*., 2018; Veith-Wolf *et al*., 2018; Meyer *et al*., 2021). In the context of Figure 2, these dielectrics can be combined with carrier-selective contact stacks so that a thin, high-quality oxide provides passivation, while an overlying doped poly-Si or TCO layer provides lateral conduction and tailored band bending.

In both silicon and perovskite technologies, the state of the art is moving toward multifunctional interfacial stacks that combine dipolar SAMs, 2D layers, and dielectric passivation. For example, inverted perovskite solar cells that use SAM-based hole-selective layers on top of $NiO_x$ or other wide-bandgap oxides have achieved very high open-circuit voltages and improved stability, illustrating the synergy between molecular dipoles and inorganic passivation (Kim *et al*., 2020; Chen *et al*., 2025; Yang *et al*., 2025). In silicon heterojunctions, textured front surfaces coated with TCO/dielectric/SAM stacks are being explored to jointly optimize anti-reflection, contact resistivity, and surface recombination.

Overall, interface engineering for light–matter control can be viewed as co-optimizing three intertwined roles: (i) chemical passivation, to suppress defects and traps; (ii) electrostatic design, using dipoles and fixed charges to sculpt band alignment and built-in fields; and (iii) photonic design, using optical spacers, refractive-index contrast, and 2D layers to manage absorption and emission. When these roles are jointly addressed, the interfaces in Figure 2 cease to be simple boundaries and become active components that help to preserve the quasi-Fermi level splitting generated in the absorber and to funnel both light and charge toward the carrier-selective contacts.

## 4. Ultrafast Carrier Dynamics: From Photon Absorption to Charge Extraction

### 4.1 Hot-Carrier Generation, Thermalization, and Cooling Pathways

When a photon with energy $h\nu > E_g$ is absorbed, electrons and holes are not born in thermal equilibrium with the lattice but in a highly non-thermal distribution, typically carrying excess kinetic energy of order $h\nu - E_g$. Ultrafast spectroscopy consistently reveals three generic stages in the subsequent evolution. First, during coherent excitation and dephasing on a femtosecond timescale, the initially created polarization decays and the carriers begin to lose memory of the driving field. Second, rapid carrier–carrier scattering redistributes energy among electrons and holes, bringing them to a hot Fermi–Dirac distribution characterized by an elevated carrier temperature. Third, these hot carriers cool toward the lattice temperature through carrier–phonon interactions, primarily by emitting longitudinal optical (LO) phonons followed by slower coupling to acoustic modes.

In conventional direct-gap semiconductors such as GaAs, and in crystalline silicon under above-bandgap excitation, carrier–carrier thermalization is extremely fast, typically occurring within about 10–100 fs. Cooling from this hot distribution down to the band edge then proceeds over roughly 0.2–2 ps through LO-phonon emission and subsequent acoustic-phonon–mediated energy loss. Under 1-sun–like excitation, this means that most carriers reach near-band-edge energies long before they have diffused more than a few nanometres, so device operation can often be described using near-equilibrium transport at the band edge.

Metal-halide perovskites, both in bulk films and as nanocrystals, deviate markedly from this picture by exhibiting anomalously slow hot-carrier cooling, especially at higher excitation fluences. Femtosecond pump–probe and transient-absorption experiments frequently report hot-carrier lifetimes extending to tens of picoseconds, far longer than in GaAs for comparable excess energies. This slowdown is generally attributed to a combination of large polaron formation, which screens carrier–phonon coupling; a hot-phonon bottleneck, in which emitted LO phonons are re-absorbed before they

can dissipate their energy; and phonon up-conversion processes that recycle vibrational energy back into the electronic system (Fu *et al*., 2017; Herz, 2016). Pressure-dependent studies on $MAPbI_3$ further show that compressing the lattice can accelerate hot-carrier cooling by roughly a factor of two above the Mott transition density, highlighting that electron–phonon coupling and lattice stiffness can be used as design parameters to tune the cooling window (Muscarella *et al*., 2021). Alloyed and mixed-metal perovskites extend this design space even further: mixed Pb–Sn compositions and low-dimensional nanocrystals often combine slow cooling with reasonably high mobilities, making them attractive testbeds for hot-carrier photovoltaic concepts (Monti *et al*., 2020).

Across all of these materials, hot-carrier dynamics are typically probed using femtosecond transient absorption and time-resolved photoluminescence, which track spectral shifts and linewidths to infer carrier temperatures; time-resolved terahertz and optical-pump/THz-probe spectroscopy, which directly measure the mobility and conductivity of hot carriers; and, in a growing number of cases, operando ultrafast measurements on complete devices that link hot-carrier cooling to internal fields and contact extraction. Together, these studies make clear that any realistic hot-carrier photovoltaic architecture must synchronize carrier extraction with the finite cooling window on the order of a few to a few tens of picoseconds in perovskites while simultaneously suppressing trap-assisted and Auger recombination that would otherwise dissipate the stored excess energy before it can be harvested.

**Table 2: Characteristic ultrafast carrier timescales in representative PV absorbers**

| Material class | Thermalization (carrier–carrier) | Hot-carrier cooling to band edge | Typical probe techniques |
|---|---|---|---|
| c-Si, GaAs (bulk) | 10–100 fs | 0.2–2 ps | TA, TRPL, TR-THz |
| Metal halide perovskites (3D) | 20–200 fs | 1–50 ps (fluence dependent) | TA, TRPL, TR-THz, 2D spectroscopy |
| Mixed Pb–Sn or low-dimensional perov. | 20–200 fs | 5–100 ps | TA, TRPL, magneto-optical probes |
| Organic donor–acceptor blends | 10–100 fs | <1 ps to CT states; few ps to band edge | TA, time-resolved EL |

### 4.2 Excitons vs Free Carriers: Binding, Dissociation, and Transport in Different Active Media

Immediately after photoabsorption, the nature of the primary excitation whether a tightly bound exciton or a nearly free electron hole pair is set by the competition between Coulomb attraction and dielectric screening. This balance is commonly quantified by the exciton binding energy $E_{\mathrm{B}}$, which scales roughly as $\mu/\varepsilon_r^2$ , where $\mu$ is the reduced effective mass and $\varepsilon_r$ the relative dielectric constant (Sugie *et al*., 2023; Yang *et al*., 2017). In classical inorganic semiconductors such as crystalline silicon and GaAs, large dielectric constants and relatively small effective masses yield Wannier–Mott excitons with binding energies of only a few meV, comparable to or smaller than $k_{\mathrm{B}}T$ at room temperature. Under solar illumination, these excitons ionize essentially instantaneously, so transport is well described in terms of free carriers undergoing drift and diffusion in the band structure. Radiative recombination and quasi-Fermi level splitting in such media can therefore be analyzed using textbook semiconductor statistics, with excitonic corrections entering primarily at low temperature or under high magnetic fields (Herz, 2016).

Organic semiconductors, by contrast, combine low dielectric constants ($\varepsilon_r \sim 3-4$) with relatively localized π–π* orbitals. This combination leads to Frenkel-like excitons with typical binding energies of 0.3–0.8 eV, well above thermal energy at room temperature (Sugie *et al*., 2023). As a result, photoexcitation produces neutral excitons that are metastable with respect to free charges and must diffuse to regions with a strong local electric field or a sharp energetic offset most often a donor–acceptor heterojunction before dissociating. Exciton diffusion lengths in state-of-the-art organic photovoltaic blends typically lie in the 5–20 nm range, with recent precision measurements emphasizing how sensitive these values are to energetic disorder, morphology, and measurement technique (Riley *et al*., 2024). Efficient organic devices therefore rely on nanoscale bulk heterojunction architectures in which the domain size is of the same order as the exciton diffusion length, so that a large fraction of excitons can reach an interface before decaying radiatively or via non-radiative channels.

Hybrid metal halide perovskites occupy an intermediate, but highly favorable, position in this landscape. Their large static dielectric constants and moderate effective masses produce Wannier-like excitons with binding energies on the order of 10–30 meV in $MAPbI_3$ and related compositions, so that at room temperature the population is dominated by free carriers, even though excitonic resonances are clearly resolved in low-temperature spectra (Yang *et al*., 2017; Soufiani *et al*., 2015). Time-resolved optical experiments show that any initially formed excitons rapidly ionize into free carriers on sub-picosecond timescales, supported by strong polaronic screening and dynamic disorder. Consequently, transport in perovskite solar

cells resembles that in high-quality inorganic semiconductors: electrons and holes diffuse with micrometre-scale diffusion lengths and can be described by effective-mass models, while excitonic effects enter mainly through subtle modifications of absorption edge shape, radiative recombination coefficients, and photon recycling (Herz, 2016; Johnston & Herz, 2016).

Dissociation and transport mechanisms also depend strongly on the interfacial energetics and dimensionality of the active layer. In organic bulk heterojunctions, charge separation is often framed in terms of Onsager–Braun physics: an exciton reaching the donor–acceptor interface forms a charge-transfer (CT) state, whose fate dissociation into free charges versus geminate recombination depends on the driving-force (energy offset between donor HOMO and acceptor LUMO), local electric field, and energetic disorder. Modern work shows that even "small-offset" systems with $\Delta E \lesssim 0.1\,eV$ can achieve efficient charge generation if exciton diffusion is long enough and the CT state is sufficiently delocalized, but such architectures become more sensitive to interfacial traps and morphology. In perovskites, by contrast, built-in fields at the perovskite/transport-layer interfaces typically separate charges without needing large band offsets, so reducing interfacial energy losses and preserving the quasi-Fermi level splitting becomes more important than driving exciton dissociation (Johnston & Herz, 2016; Wang *et al*., 2021).

Across these material classes, the competition between exciton binding, dissociation, and transport sets the microscopic routes by which photogenerated energy is converted into extractable charge. Organic absorbers exemplify an exciton-limited regime in which optimizing exciton diffusion length, interfacial energetics, and nanoscale morphology is essential for minimizing geminate and non-geminate losses (Riley *et al*., 2024; Sugie *et al*., 2023). Perovskites and classical inorganics, in contrast, operate in a predominantly free-carrier regime in which the key figures of merit become mobility, diffusion length, and the suppression of non-radiative recombination at defects and interfaces. A unified description of ultrafast carrier dynamics therefore has to explicitly track which regime a given absorber occupies, since the relevant design levers for device optimization dielectric engineering, dimensionality, nanostructuring, or interface energetics depend sensitively on whether the primary excitation is an exciton or a free electron–hole plasma.

### 4.3 Recombination Channels: Radiative, Shockley–Read–Hall, and Auger Processes in Advanced PV

Once excitons have dissociated or free carriers have been generated directly, their subsequent fate is governed by a hierarchy of recombination channels. In the radiative limit, electrons and holes recombine by emitting photons whose spectrum mirrors the semiconductor's absorption edge. This purely radiative band-to-band recombination sets the Shockley–Queisser limit and is described via a radiative recombination coefficient BBB, which depends on the joint density of states, transition matrix elements, and optical environment (Kirchartz & Rau, 2018). In direct-gap materials such as GaAs, large optical matrix elements and strong absorption lead to relatively high radiative rates. In indirect-gap materials like crystalline silicon, by contrast, phonon assistance is required, suppressing BBB and making radiative processes slow compared to non-radiative channels under typical device conditions (Fell *et al*., 2021). Hybrid perovskites fall between these extremes: although nominally direct-gap, they may exhibit a slightly indirect character and strong photon recycling, which effectively reduces the radiative coefficient relevant for open-circuit conditions while still enabling high external luminescence yields in optimized devices (Johnston & Herz, 2016; deQuilettes *et al*., 2019).

Real photovoltaic absorbers, however, seldom operate in the ideal radiative limit. Defects, impurities and imperfect interfaces introduce localized states in the band gap that mediate Shockley–Read–Hall (SRH) recombination. In the classic SRH picture, recombination proceeds via sequential capture of electrons and holes into a defect level at energy $E_{\mathrm{T}}$, with rates set by capture cross sections, thermal velocities, and trap densities (Shockley & Read, 1952). Mid-gap defects are particularly detrimental because they maximize the SRH recombination rate at a given carrier concentration, thereby shortening the minority-carrier lifetime and reducing the open-circuit voltage. Modern loss analyses across III–V, Si, organic, and perovskite devices consistently show that to approach within 1% of the internal radiative efficiency limit, SRH lifetimes must reach the microsecond–millisecond range, which constrains the allowable defect densities to $10^{12}\,\mathrm{cm}^{-3}$ depending on cross sections and operating injection levels (Nakamura *et al*., 2020; Kirchartz & Rau, 2018).

In perovskite solar cells, trap-assisted recombination is still the dominant non-radiative loss channel in many architectures, even though trap densities are already lower than in typical organic or thin-film inorganic absorbers. Time-resolved photoluminescence, transient photovoltage, and impedance spectroscopy measurements consistently point to deep-defect and interfacial states as key recombination centres, particularly at grain boundaries and at the perovskite/transport-layer interfaces (deQuilettes *et al*., 2019; Wang *et al*., 2021). Chemical passivation strategies—such as Lewis-base additives, alkali halide treatments, or self-assembled monolayers—have been shown to increase effective SRH lifetimes by one to two orders of magnitude, translating directly into improved open-circuit voltages and fill factors. Similar interface-engineering ideas carry over to silicon heterojunctions and tandem devices, where high-quality amorphous passivation layers and carefully tuned contact stacks are

required to keep SRH current densities below a few fA · $cm - 2^{-2}$.

Auger recombination constitutes a third, intrinsically non-radiative channel that becomes important at high carrier concentrations, for example under concentrated sunlight, in thick high-doping regions, or near the maximum power point of high-efficiency devices. In a band-to-band Auger process, the energy released when an electron and hole recombine is transferred to a third carrier, which is excited to a higher energy within the same band. The rate therefore scales as $Cn^2p\ or\ Cnp^2$, depending on which carriers dominate, where C is the Auger coefficient. In crystalline silicon, Auger recombination is a major efficiency limiter at high injection, and accurate parameterizations of C as a function of doping and injection level have been crucial for reliably predicting the ultimate efficiency limits of advanced cell designs (Richter *et al*., 2012). Recent reassessments of intrinsic recombination in silicon further highlight that Auger losses, together with radiative processes and photon recycling, fully determine the achievable voltage once extrinsic SRH contributions are minimized (Niewelt *et al*., 2022; Fell *et al*., 2021).

In halide perovskites and wide-bandgap III–V materials, Auger recombination frequently appears in a more complex, defect-assisted variant. Here, a localized trap participates as one of the three states involved in the process, leading to "trap-assisted Auger" or "Auger–Meitner" kinetics that can mimic bimolecular recombination over a broad range of carrier densities (Staub *et al*., 2018). Simulations and experiments on mixed-cation perovskites show that even modest Auger capture coefficients can significantly depress the open-circuit voltage and fill factor when trap densities remain above $10^{14}\,\mathrm{cm}^{-3}$, particularly under concentrated illumination or in thick active layers (Hossain *et al*., 2023; Baloch *et al*., 2018). For multi-junction and tandem architectures, where top cells often operate at higher effective concentrations, managing Auger coefficients through band-structure engineering and careful doping control becomes a critical design lever.

From the perspective of ultrafast carrier dynamics, these recombination channels unfold over very different timescales. Radiative recombination lifetimes can range from nanoseconds in high–radiative-efficiency III–V materials to microseconds or longer in indirect-gap or strongly photon-recycling systems. SRH lifetimes span from sub-nanosecond in defect-rich films to the microsecond–millisecond regime in state-of-the-art perovskites and silicon heterostructures with carefully passivated surfaces (Johnston & Herz, 2016; deQuilettes *et al*., 2019). Auger processes are typically negligible at low injection but can dominate on sub-nanosecond timescales once carrier densities approach $10^{18}\,\mathrm{cm}^{-3}$. For advanced PV, "approaching the radiative limit" thus means simultaneously suppressing SRH and trap-assisted Auger recombination, while accepting a residual, well-understood radiative and intrinsic Auger loss floor. In the broader context of this review, these recombination pathways form the final stage in the ultrafast sequence that begins with photon absorption and hot-carrier relaxation: they determine how long quasi-Fermi level splitting can be sustained and, therefore, how much of the initially absorbed photon energy can ultimately be harvested as electrical work.

## 5. Ultrafast Spectroscopy as a Probe of Light–Matter Interactions

### 5.1 Transient Absorption, Time-Resolved PL, and THz Spectroscopy for PV Materials

TA, TRPL and TRTS form a complementary triad for characterizing carrier dynamics in advanced PV absorbers. In TA, a femtosecond pump pulse excites the sample and a delayed broadband probe measures the differential transmission or reflectance ΔA(t,λ). Ground-state bleach, stimulated emission and excited-state absorption features track the population of electronic states and their energy relaxation pathways, enabling direct observation of hot-carrier cooling, state filling and charge transfer to transport layers (Ponseca Jr. *et al*., 2016; Monti, 2020). In perovskite solar cells, TA has mapped sub-picosecond carrier generation, polaron formation and interfacial charge transfer to electron and hole transport layers, as well as slow nanosecond tail dynamics associated with traps and grain boundaries (Chen *et al*., 2024; Srivastava *et al*., 2023).

TRPL monitors the time-dependent spontaneous emission following pulsed excitation, giving direct access to radiative and non-radiative recombination channels. By varying excitation density, researchers separate mono-, bi- and Auger recombination contributions, fit rate equations and extract effective recombination coefficients and charge-carrier lifetimes (Peters *et al*., 2019; Bowman *et al*., 2022). In perovskites and other PV absorbers, TRPL studies have shown that increasing material quality and interface passivation can push effective lifetimes into the microsecond regime, consistent with quasi-radiative operation at open circuit (Ning *et al*., 2018; Ochoa *et al*., 2022).

TRTS or optical pump–THz probe spectroscopy completes the picture by measuring the complex photoconductivity σ(ω,t) with sub-picosecond resolution. A THz pulse probes how photocarriers respond to an oscillating electric field, allowing extraction of carrier mobility, scattering times and localization via Drude or Drude–Smith models (Hempel *et al*., 2022; Cinquanta *et al*., 2019). In perovskite thin films and nanocrystals, TRTS has revealed high mobilities, polaronic effective masses and how trapping or phase segregation reduces the mobile carrier fraction (Ponseca Jr. *et al*., 2016; Gatto *et al*., 2021). The combination of TA, TRPL and TRTS thus provides a multi-dimensional view of carrier generation,

thermalization, transport and recombination in PV materials across 12–15 orders of magnitude in time.

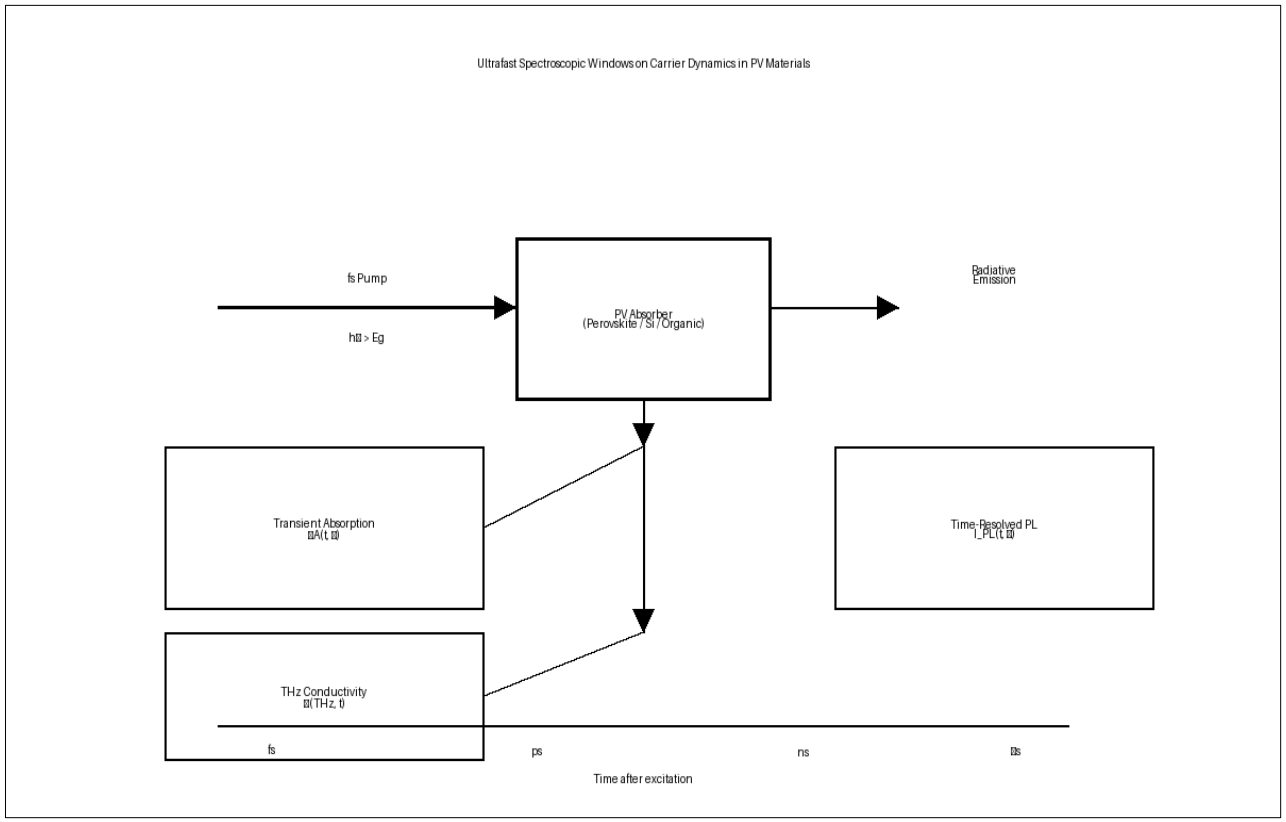


**Figure 3: Ultrafast Spectroscopic Windows on Carrier Dynamics in Perovskite Solar Cells.**

Dynamical processes in a perovskite solar cell, from charge generation and relaxation to extraction, transport, recombination and collection. Time-scale dial from femtoseconds to milliseconds, with each process mapped onto its characteristic window.Table of measurement techniques (TA, TRPL, TRTS and related methods) assigned to each process, highlighting how their combination reconstructs the complete carrier-dynamics picture.

### 5.2 Probing Buried Interfaces and Heterostructures: Pump–Probe and Time-Resolved Microscopy

Standard ultrafast measurements average over the illuminated volume and are often dominated by the bulk response. However, in thin-film and heterostructure PV devices, key loss channels originate at buried interfaces, transport layers and grain boundaries that occupy a small fraction of the volume but strongly influence performance (Pu *et al*., 2023; Srivastava *et al*., 2023). To access these regions, researchers have developed spatially resolved pump–probe and time-resolved microscopy techniques.

Time-resolved PL microscopy (TRPLM) images the spatiotemporal evolution of photoluminescence with sub-micrometre resolution, allowing direct visualization of carrier diffusion, trapping and non-radiative recombination at grain boundaries, interfaces and inclusions (Ochoa *et al*., 2022; Jariwala *et al*., 2019). By fitting the broadening of PL spots over time to diffusion models, one can extract local diffusivities and observe how grain boundaries either block carriers or, in optimized films, act as transport channels (Ning *et al*., 2018; Gatto *et al*., 2021; Chen *et al*., 2024). Transient absorption microscopy and near-field optical pump–probe variants extend these ideas to non-emissive states and deeply buried interfaces, using contrast from excited-state absorption or local refractive-index changes.

A recent wave of work has focused specifically on buried charge-selective interfaces in perovskite solar cells, where non-radiative recombination and trapped carriers can strongly limit open-circuit voltage and fill factor. Time-resolved spectroscopies that selectively excite or probe near the interface—using wavelength, incidence angle or waveguiding effects—have revealed nanosecond to millisecond trapped-carrier dynamics and identified interfacial passivation strategies that recover radiative behaviour (Hu *et al*., 2025; Khan *et al*., 2024). When combined with spatial mapping, these methods provide a “defect cartography” of buried interfaces and heterostructures, guiding engineering of transport layers, passivation molecules and compositional grading.

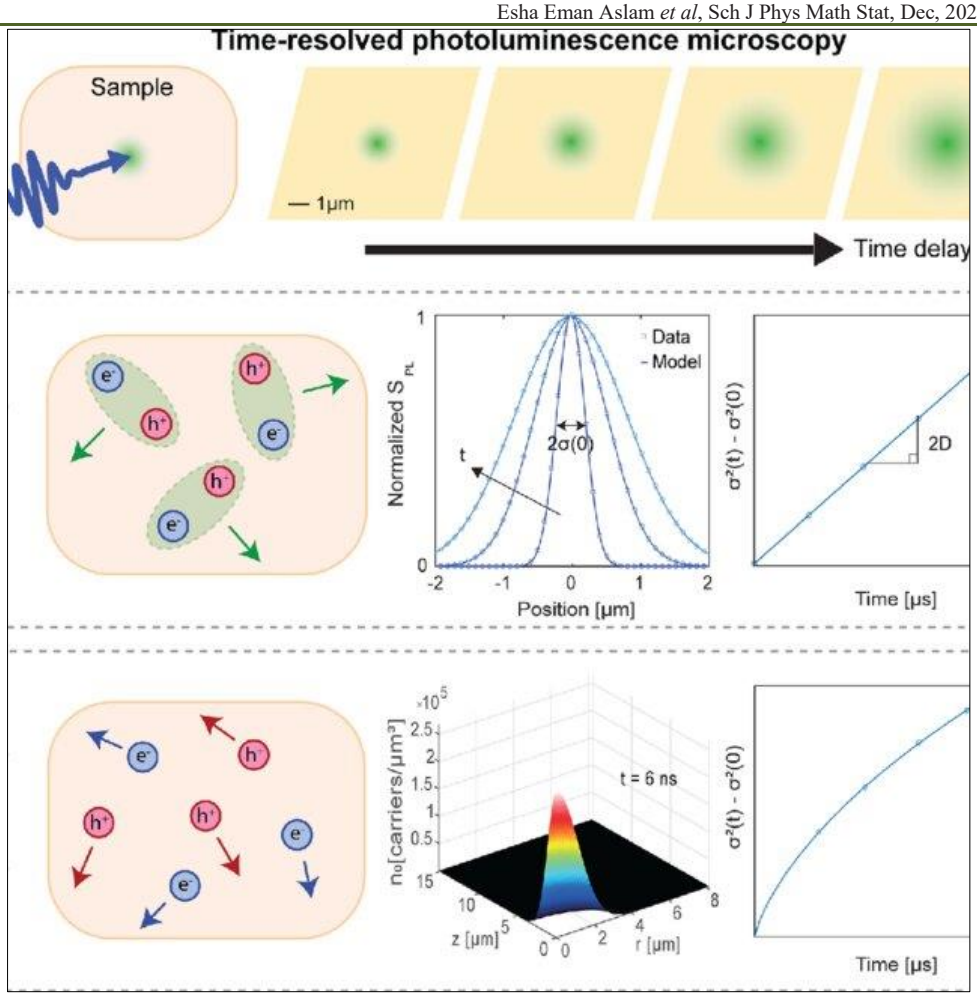


**Figure 4: Time-Resolved Photoluminescence Microscopy of Carrier Diffusion in Thin-Film Absorbers**

Illustration of transient/time-resolved PL microscopy where a localized excitation spot broadens with time delay while the PL amplitude decays, capturing the coupled action of diffusion + recombination. Successive-delay spatial line profiles are fit (e.g., Gaussian/variance growth) to extract diffusivity (D) and an effective lifetime, and the plot of mean-squared displacement vs time shows how different regimes appear (approximately linear growth for diffusion-dominated transport; deviations/curvature when recombination kinetics, nonlinear PL–density scaling, or localized quenching become important.

### 5.3 Extracting Device-Relevant Quantities: Lifetimes, Mobilities, Diffusion Lengths, and Rate Constants

While ultrafast measurements yield rich time- and wavelength-dependent signals, their ultimate value for photovoltaics lies in extracting quantitative parameters that can feed into drift–diffusion or equivalent-circuit simulations. For TRPL and TA, this typically involves fitting kinetic models rate equations for carrier populations that include radiative, Shockley–Read–Hall and Auger terms to the measured decays as a function of excitation density (Peters *et al*., 2019; Bowman *et al*., 2022). By combining quantum-efficiency data with time-resolved measurements, one can disentangle absolute radiative and non-radiative rates, providing a direct measure of internal luminescence efficiency and quasi-Fermi level splitting under operating conditions.

Carrier mobilities and scattering times are extracted from TRTS by fitting the complex photoconductivity to Drude or Drude–Smith models, sometimes extended to account for polaronic effects or localization (Cinquanta *et al*., 2019; Hempel *et al*., 2022; Ponseca Jr. *et al*., 2016). Once both mobility μ and effective lifetime τ are known, diffusion lengths follow from $L = \sqrt{D\tau}\ with\ D = \mu k_B T/q$. For perovskites, such analyses have revealed diffusion lengths of tens to hundreds of micrometres in high-quality single crystals and optimized polycrystalline films, consistent with their exceptional photovoltaic performance (Ning *et al*., 2018; Hodes, 2015).

Spatially resolved techniques refine these estimates by providing local parameters rather than global averages. TRPL microscopy and related methods can be inverted to yield diffusivities and lifetimes as a function of position, using robust fitting strategies that account for finite instrument response and complex geometries (Robust Estimation of Charge Carrier Diffusivity, 2022; Ochoa *et al*., 2022). These local values

feed directly into models of grain-boundary resistance, interface recombination velocities and lateral transport in modules. New interfacial spectroscopies that monitor trapped carriers at buried interfaces extend this parameter set to include trap densities, capture cross sections and detrapping times (Hu *et al*., 2025; Khan *et al*., 2024).

Ultimately, a consistent workflow emerges: TA and TRPL define radiative and non-radiative rate constants; TRTS provides mobilities and carrier effective masses; and spatially resolved variants distribute these parameters across grains and interfaces. When fed into physically realistic device simulations, this hierarchy of quantities allows one to predict open-circuit voltage, fill factor and efficiency from spectroscopic data alone, closing the loop between ultrafast light–matter interaction and steady-state PV performance (Hempel *et al*., 2022; Srivastava *et al*., 2023).

## 6. Nanophotonics and Metasurfaces for Optical Field Engineering

### 6.1 Plasmonic vs Dielectric Nanostructures: Light Trapping, Scattering, and Parasitic Losses

Plasmonic nanostructures exploit the collective oscillation of free electrons in metals—localized surface plasmon resonances (LSPRs) in nanoparticles and surface plasmon polaritons (SPPs) at metal dielectric interfaces to concentrate optical fields into deep-subwavelength volumes. When integrated into solar cells (e.g., as front nanoantennas, rear gratings, or embedded particles), they can strongly scatter incident light into guided modes, extend the optical path length in ultrathin absorbers, and even selectively enhance specific spectral bands (e.g., near the band edge of organic or perovskite absorbers) (Hsiao *et al*., 2012; Erwin *et al*., 2016; Subhan *et al*., 2025).

However, metallic strategies carry an intrinsic trade-off: the same enhanced near fields that boost absorption in the semiconductor also drive Ohmic losses in the metal. For noble metals like Au and Ag, this parasitic absorption can become substantial in the visible, reducing the net current gain, especially when metal coverage or overlap with the active region is high (Maier, 2007; Dunbar *et al*., 2012). Ageing, diffusion, and chemical instability of metal nanoparticles under operation further complicate long-term stability. Consequently, plasmonics tends to be most beneficial in niche regimes very thin absorbers, spectrum-selective designs, or architectures where metals can be spatially separated from the highest-field regions.

Dielectric nanostructures instead use high-index, low-loss materials (e.g., Si, $TiO_2$, GaP, $Si_3N_4$) to support Mie-type resonances that combine electric and magnetic dipoles, enabling strong scattering and local field enhancement with negligible absorption in the structure itself (Brongersma *et al*., 2014; Amalathas & Alkaisi, 2019; Ju *et al*., 2023). These resonant scatterers or textures can:

- Suppress front-surface reflection across broad spectra via graded effective refractive index.
- Couple light into lateral waveguide modes and higher-order resonances that increase path length in thin films.
- Shape the angular distribution of light inside the absorber, approaching or surpassing classical Yablonovitch-type limits in the nanophotonic regime (Yu *et al*., 2010; Yu *et al*., 2011).

Because dielectric nanophotonics largely avoids Ohmic losses, it is now generally preferred for high-efficiency, large-area solar technologies, with plasmonics reserved for specialized functionalities (e.g., upconversion, infrared harvesting, or local field-enhanced chemistry at electrodes). Table 6.1 summarizes the main contrasts.

**Table 3: Plasmonic vs dielectric nanostructures for light trapping in PV devices**

| Aspect | Plasmonic nanostructures | Dielectric nanostructures |
|---|---|---|
| Typical materials | Au, Ag, Al, Cu | Si, $TiO_2$, GaP, $Si_3N_4$, oxides, nitrides |
| Dominant resonances | LSPRs, SPPs (free-electron plasmon modes) | Mie-type electric & magnetic multipoles |
| Main mechanism | Near-field enhancement, strong scattering into modes | Low-loss scattering, effective-index grading, mode coupling |
| Spectral tunability | Strong, via size/shape/embedding medium | Strong, via geometry and index contrast |
| Parasitic absorption | High (Ohmic losses in metal) | Very low (bandgap-above operation) |
| Stability considerations | Diffusion, oxidation, morphology evolution | Often compatible with existing dielectric stacks |
| Best suited use-cases | Ultrathin cells, localized enhancements, upconversion | Broadband light trapping, AR coatings, tandem integration |
| Integration challenges | Metal–semiconductor quenching, contact design | Nano-fabrication tolerances, pattern transfer |

### 6.2 Metasurface Architectures for Spectral, Angular, and Polarization Control

Metasurfaces are 2D arrays of subwavelength "meta-atoms" that impart tailored amplitude, phase, and polarization responses to incident light. In PV, metasurfaces can serve as multifunctional front or rear optics that simultaneously reduce reflection, steer light into high-absorption modes, and control the angular and polarization dependence of both absorption and emission (Mascaretti *et al*., 2023; Brongersma *et al*., 2014).

Spectral Control and Broadband Absorption Broadband solar absorbers based on metasurfaces use multi-resonant nanoantennas, graded period distributions, or a-periodic patterns to achieve near-unity absorption over the solar spectrum. All-metal or metal–dielectric metasurface absorbers have demonstrated >90–97% absorption across the visible and near-infrared using simple disk or elliptical nanoantenna arrays on metal back reflectors, while maintaining low aspect ratio for manufacturability (Wu *et al*., 2025; Ashrafi-Peyman *et al*., 2024). In solar cells, similar concepts can be used either as stand-alone thermal absorbers (e.g., thermophotovoltaics) or as "photon funnels" that couple broadband sunlight into a thinner semiconductor.

Angular Control and Wide-Acceptance Optics Metasurfaces can also shape the angular response of PV devices. Designs with weakly angle-dependent resonances can maintain high absorption up to large incidence angles (>70–80°), which is critical for stationary modules without sun tracking (Huettenhofer, 2022; Chen *et al*., 2018). Conversely, angularly selective metasurfaces can restrict the escape cone of luminescent photons, improving photon recycling and VOC while still allowing efficient in-coupling of sunlight from relevant angles—a concept that directly connects metasurface design to reciprocity-governed efficiency limits (Rau, 2014; Yu *et al*., 2010).

Polarization Engineering. Although sunlight is essentially unpolarized, polarization-insensitive metasurfaces ensure robust performance under real-world conditions, while polarization-selective designs are useful for integrated optics and tandem architectures where different polarizations may be directed into different subcells. Recent reviews of polarization-controlling metasurfaces highlight the use of anisotropic meta-atoms (e.g., nanorods, split-ring resonators, rotated dielectric bricks) to realize quarter-wave plates, polarization rotators, and spin-selective responses over broad bandwidths (Khan *et al*., 2025).

**Table 4: Representative metasurface architectures for PV-relevant optical control**

| Metasurface function | Typical architecture / meta-atoms | Design features | PV-relevant benefit |
|---|---|---|---|
| Broadband antireflection & absorption | Metal or dielectric nanodisks / nanocones on back mirror | Multi-resonant, subwavelength period, low aspect ratio | Reduced front reflection, enhanced path length |
| Spectrum splitting / color-selective | Dispersive gratings, phase-gradient metasurfaces | Spatially varying phase to separate wavelengths | Direct different spectral bands to tandem subcells |
| Angularly robust absorbers | Quasi-random or gradient-period metasurfaces | Weak angle dependence of resonances | High absorption over large incidence angles |
| Angularly selective emitters/absorbers | Leaky-mode or guided-mode metasurfaces | Narrow angular transmission/emission windows | Reduced emission losses, improved photon recycling |
| Polarization-insensitive light trapping | Symmetric meta-atoms (disks, squares) | Rotational symmetry | Uniform performance for unpolarized sunlight |
| Polarization-control metasurfaces | Anisotropic rods, split-rings, rotated bricks | Birefringence, geometric phase (Pancharatnam–Berry phase) | Tailored polarization for integrated optoelectronics |
| Bifacial / tandem coupling metasurfaces | Double-sided meta-optics, interlayer metasurfaces | Different responses for front vs rear illumination | Improved utilization of diffuse and albedo light |

### 6.3 Photon Recycling, Emission Engineering, and Reciprocity-Based Device Optimization

High-performance solar cells must not only absorb light efficiently; they must also manage *emission* efficiently. In the radiative limit, any recombination event produces a photon, and a fraction of these photons is re-absorbed within the device—a process known as photon recycling. When radiative recombination dominates and parasitic optical losses are minimized, photon recycling increases the quasi-Fermi level splitting and hence the open-circuit voltage and maximum power point voltage (Raja *et al*., 2021; Brenes *et al*., 2019).

Metal halide perovskites are exemplary in this regard: they combine strong absorption, sharp band edges, and long non-radiative lifetimes, enabling sizable internal radiative efficiencies and measurable photon-recycling effects even at moderate thickness (Cho *et al*., 2021; Zeder *et al*., 2022; Bowman *et al*., 2020). Optical and electrical modelling indicate that under realistic

conditions, photon recycling can boost the maximum-power-point voltage by tens of millivolts, translating into several absolute percentage-points of power conversion efficiency—*provided* that optical design suppresses parasitic absorption in transport layers, electrodes, and textured interfaces (Raja *et al*., 2021; Brenes *et al*., 2019).

Rau's thermodynamic framework for light management formalizes these ideas by relating the open-circuit voltage to an ideal radiative limit minus entropy-producing losses from imperfect light trapping, parasitic absorption, and non-radiative recombination (Rau, 2014). In this picture, optimizing a device means maximizing its external radiative efficiency (ERE)—the fraction of recombination events that yield photons escaping the device—while also maximizing the probability that escaped photons are re-directed back into useful optical paths by mirrors, textured interfaces, or metasurfaces. DeQuilettes and co-workers showed that systematically improving ERE in perovskite devices (via defect passivation, better contacts, and reduced parasitic absorption) correlates strongly with record-low voltage losses and near-radiative-limit behavior (deQuilettes *et al*., 2020).

Reciprocity principles provide a powerful design rule: the same optical structure that enhances *absorption* of sunlight at a given wavelength and angle will, in reverse, enhance *emission* into those channels under electrical injection or photogenerated carrier populations. Thus, metasurfaces and nanophotonic textures must be engineered to:

- Trap sunlight efficiently over the desired angular and spectral range,
- Limit parasitic absorption of both incident and re-emitted photons, and
- Shape the emission pattern to maximize useful photon recycling and external luminescence while respecting module-level constraints.

Photon-recycling-aware nanophotonic design often favors high-index dielectric structures and reflective mirrors that keep luminescent photons within the absorber, combined with angular-selective elements that narrow the escape cone, thereby reducing entropy generation in the emission process (Yu *et al*., 2010; Rau, 2014; Raja *et al*., 2021). Table 6.3 summarizes representative strategies.

## 7. Laser-Enabled Photonic Structuring and Laser–Material Processing

### 7.1 Laser–Material Interaction Regimes: ns, ps, and fs Processing of PV Films

In the **nanosecond regime**, the laser pulse duration is much longer than the electron–phonon relaxation time, so deposited energy largely thermalizes during the pulse. Heat diffuses over a characteristic thermal diffusion length $L_{th} \sim \sqrt{4\kappa\tau}$, leading to melting, resolidification and a relatively wide heat-affected zone (HAZ). For PV manufacturing, ns lasers are widely used for P1–P2–P3 scribing in CIGS, CdTe and perovskite modules, where efficient ablation and throughput outweigh the need for ultraclean edges (Jamaatisomarin *et al*., 2023; Huang *et al*., 2024; Nanosecond Laser Scribing of CIGS, 2018). Typical applications include: P1 scribing of the front transparent conducting oxide (TCO), P2 interconnect scribing through absorber layers, and P3 back-contact isolation, often with 1064–532 nm ns sources.

Picosecond lasers shorten the interaction time and reduce heat diffusion, partially decoupling energy deposition from lattice heating. Experiments on $WO_x$, $VO_x$ and $MoO_x$ passivating films on crystalline silicon show that ps pulses can cleanly remove transition-metal oxides at fluences where ns pulses already damage the underlying Si, yielding a wider "process window" between ablation onset and substrate damage (Muñoz García *et al*., 2022). Picosecond scribing of ITO and AZO TCOs likewise improves edge quality, reduces micro-debris and narrowing of HAZ compared to ns processing, which is attractive for high-resolution P1 lines in narrow-pitch modules (Zuo *et al*., 2025; Jamaatisomarin *et al*., 2023).

In the femtosecond regime, pulse durations are shorter than the electron–phonon coupling time, so energy is initially deposited in the electronic subsystem. If fluence exceeds the ablation threshold within tens to hundreds of femtoseconds, material removal and phase change can occur before significant thermal diffusion—often described as "cold ablation" (Varlamov *et al*., 2024; Banik *et al*., 2025). Fs pulses are particularly suited to:

- Fabricating LIPSS and sub-wavelength nanostructures for light trapping with minimal HAZ.
- Precision scribing of multilayer stacks where underlying layers must remain pristine.
- Local phase transformation (e.g., a-Si → nc-Si nanopillars) with controlled crystallinity and surface passivation (Dostovalov *et al*., 2020).

Recent comparative work on ns vs ps processing of silicon and TCOs suggests that ns sources remain cost-effective for large-area scribing and doping, whereas ps/fs tools enable higher fidelity and smaller pitch—important for tandem or micro-module architectures (Rebegea, 2018; Nanosecond vs Picosecond JAP, 2025).

**Table 5: Qualitative comparison of ns, ps and fs laser regimes for PV-relevant processing**

| Pulse regime | Typical PV uses | Interaction characteristics | Advantages | Limitations / risks |
|---|---|---|---|---|
| Nanosecond | P1–P2–P3 scribing, large-area ablation | Strong thermal diffusion, melting, resolidification | High throughput, robust, mature tech | Wider HAZ, more debris, risk of delamination |
| Picosecond | Fine scribing of TCO/TMO, micro-pattern | Reduced HAZ, partial non-thermal contributions | Cleaner edges, larger process window | Higher tool cost, tighter alignment |
| Femtosecond | LIPSS, nano-texturing, precision drilling | Strongly non-thermal, "cold" ablation, self-organization | Sub-wavelength features, minimal damage | Complex beam handling, lower throughput |

### 7.2 LIPSS, Direct Writing, and Interference Patterning

Laser-induced periodic surface structures (LIPSS) emerge when a surface is irradiated near the ablation threshold by linearly polarized ultrashort pulses. Interference between the incident field and surface-scattered waves leads to self-organized ripples with periods close to, or smaller than, the laser wavelength (Müller *et al*., 2016; Balachninaitė *et al*., 2025). For PV applications, LIPSS on silicon, diamond and metals have been shown to:

- Reduce reflectance via hierarchical micro-/nano-texturing, acting as broadband anti-reflection surfaces.
- Increase light trapping by coupling incident light into guided and quasi-random modes (Light Trapping by Light Treatment, 2020).
- Drive local phase transitions, such as transforming amorphous Si into nanocrystalline Si nanopillars with conformal $SiO_2$ passivation, thereby simultaneously improving optical and electronic properties (Dostovalov *et al*., 2020).

In perovskite and organic PV, fs-LIPSS on glass or TCO substrates can create sub-wavelength relief that acts as a "photon funnel," enhancing absorption without invasive processing of the fragile active layer. Early studies also explore LIPSS on transport layers like $TiO_2$ or $SnO_2$ to modulate local field intensity and charge extraction pathways (Song *et al*., 2025).

Direct laser writing uses a focused beam scanned across the surface to define arbitrary 2D or 3D patterns. In PV, direct writing has been applied to:

- Form interdigitated back-contact patterns and local openings in passivation layers.
- Write conductive tracks or isolation lines in flexible modules.
- Pattern selective absorber removal in tandem architectures, enabling monolithic series interconnection without photolithography (Carlson, 2012; Jamaatisomarin *et al*., 2023).

By shaping the beam (e.g., Bessel, Airy or cylindrical lens geometries) and tuning scan strategies, direct writing can generate quasi-1D gratings, 2D lattices or quasi-random patterns that mimic metasurfaces, but produced in a single processing step.

Interference and holographic patterning represent a complementary approach: two or more coherent beams form a stationary interference pattern that simultaneously exposes large areas. In laser interference lithography (LIL), the resulting periodic intensity distribution is transferred into resists or directly into photo-sensitive layers, defining gratings, photonic crystals or metasurface-like structures over centimetre scales (Müller *et al*., 2016). Combining LIL with etching or lift-off enables cost-effective fabrication of diffractive couplers, spectrum-splitting gratings and angular-selective surfaces for PV modules, without scanning a focused beam.

### 7.3 Laser-Assisted Doping, Contact Formation, Defect Healing, and Local Phase/Strain Engineering

Beyond geometrical structuring, lasers can locally modify composition, doping and defect states, enabling highly selective electrical and optoelectronic engineering.

In crystalline silicon technology, laser doping and laser-fired contacts (LFC) have become key for advanced PERC/PERT and n-type cell concepts. In laser doping, a dopant source (e.g., spin-on, doped dielectric, or doped paste) is locally melted with a laser pulse, allowing rapid in-diffusion and formation of heavily doped regions (Molpeceres *et al*., 2012; Review of Laser Doping, 2025). LFCs use a similar principle to form local rear contacts: through a thin passivation dielectric, a laser pulse melts the underlying Si and metal stack, creating a small contact "spike" while preserving passivation elsewhere (Yen, 2016; Carlson, 2012; Chang *et al*., 2022). Properly optimized LFCs significantly reduce rear-surface recombination by confining high recombination to small contact points, while preserving low surface recombination velocity on the passivated areas (Muñoz García *et al*., 2022; Laser-Fired Contact for n-type Si, 2014).

In thin-film technologies, laser-assisted doping and contact formation similarly offer maskless, selective processing. Nanosecond laser scribing and local melting can activate dopants in TCOs, TMO passivation layers

or CIGS/CdTe back contacts, while simultaneously defining isolation trenches (Huang *et al*., 2024; Ishteev *et al*., 2024).

For perovskite solar cells, laser processing is emerging as a powerful tool to tune crystallization, heal defects and engineer interfaces without exposing films to prolonged thermal budgets. Recent work shows that scanned laser annealing under ambient conditions can rapidly convert wet perovskite precursors into highly crystalline films, while avoiding degradation pathways observed in conventional furnace or hot-plate annealing (Chu *et al*., 2025; Song *et al*., 2025). Pulsed laser annealing combined with 2D $MoS_2$ doping has been reported to improve carrier extraction, reduce non-radiative recombination and enhance operational stability, by simultaneously enlarging grain size and passivating grain boundaries (Sun *et al*., 2023).

Laser-induced defect healing can proceed through several mechanisms: local heating that activates diffusion of passivating species; phase re-ordering (e.g., from defect-rich to defect-poor phases); or controlled volatilization of unstable components followed by replenishment from a capping layer. In lead-halide perovskites, where halide vacancies and surface under-coordination dominate non-radiative loss, such laser-assisted treatments are particularly attractive for in-line repair of partially degraded modules (Ye *et al*., 2021; Khadka *et al*., 2024).

**Finally, fs/ps lasers can induce local phase and strain engineering**:

- Driving amorphous-to-crystalline transitions in Si and chalcogenides via controlled melt–recrystallization, as demonstrated in LIPSS-templated nc-Si nanopillars with favourable optical response (Dostovalov *et al*., 2020).
- Introducing residual tensile or compressive strain fields that shift bandgaps or tune carrier effective masses, potentially valuable for band-edge engineering in tandem cells or photonic-crystal absorbers (Banik *et al*., 2025; Balachninaitė *et al*., 2025).

Taken together, these laser-enabled processes form a toolbox for co-designing optics, electronics and mechanics at the device level: light-trapping textures, selective contacts, local passivation and bandgap/strain landscapes can now be written or rewritten directly into PV modules with micron-scale precision and industrially relevant throughputs.

## 8. Thin-Film Fabrication, Passivation, and Laser-Integrated Process Flows

### 8.1 Low-Temperature and Scalable Thin-Film Deposition (Solution, Vapor, and Hybrid Routes)

Solution-based coating. Lab-scale perovskite solar cells are still dominated by spin coating, but essentially all scalable routes replace spin with *blade*, *slot-die*, *spray* or *inkjet* coating, often at temperatures below 150 °C. Blade-coating of all functional layers except electrodes has been demonstrated with low thermal budget, achieving uniform films over several square centimetres while preserving device efficiencies above 18 %. Reviews of spray-coating emphasize that perovskites can be crystallized from solution by mild thermal annealing or gas-assisted drying, and summarize process windows for droplet size, substrate temperature and gas-knife conditions that are compatible with large-area modules.

Slot-die and R2R printing. Slot-die coating is now considered the most R2R-compatible deposition method for perovskite modules, offering low material waste, precise thickness control and straightforward integration into continuous lines. Fully slot-die-coated devices on rigid substrates have reached stabilized efficiencies around 18 %, while flexible, fully R2R-printed perovskite cells already exceed 13 % under ambient processing. Mechanism-informed R2R/roll-to-sheet slot-die systems emphasise uniform wet-film profiles, solvent-engineering to avoid ribbing, and synchronized drying zones, which together enable high-coating speeds without sacrificing morphology.

Vapor and hybrid routes. Vapor-based methods (thermal evaporation, co-evaporation, CVD) remain central to CdTe, CIGS and some all-inorganic perovskite processes, providing dense, pinhole-free films and excellent uniformity over large areas. Hybrid solution–vapor approaches—for example, slot-die coating of $PbI_2$:CsI precursor films followed by vapor or gas-phase conversion to perovskite—offer tighter control of crystal growth and stoichiometry, improving stability and reducing Pb waste. These hybrid routes are especially attractive for tandems on textured Si, where conformal coverage over rough substrates is required.

**Table 6: Representative low-temperature, scalable deposition routes for thin-film PV**

| Route / method | Typical materials | Substrates | Key features | Scale potential |
|---|---|---|---|---|
| Spin coating | Perovskites (lab), organics | Small rigid (glass/Si) | Excellent control; not scalable; high material waste | Research/screening only |
| Blade coating | Perovskites, transport layers | Glass, flexible glass | Simple hardware, meter-scale coating, low temp | Sheet-to-sheet; proto-R2R |
| Slot-die coating | Perovskites, organics, TCOs | Plastic foils, glass | Precise thickness; low waste; inline drying; R2R-ready | High (roll-to-roll and roll-to-sheet) |

| | | | | |
|---|---|---|---|---|
| Spray coating | Perovskites, oxides | Textured, 3D surfaces | Conformal on rough surfaces; parameter-rich | Medium–high (with process control) |
| Inkjet printing | Perovskites, organics | Small/medium-area | Digital patterning; materials-efficient | Module interconnects, patterned stacks |
| Vapor deposition | CdTe, CIGS, some perovskites | Glass, metal foils | Dense films; excellent uniformity; higher capex | Industrial thin-film modules |
| Hybrid solution–vapor | Perovskites | Textured Si, foils | Controlled crystallization; reduced waste | Emerging for tandems & modules |

### 8.2. Chemical, Field-Effect, and Photonic Passivation in Thin-Film Devices

In thin-film and tandem devices, passivation must simultaneously address electronic defects, interfacial band alignment and optical losses. Three complementary levers chemical, field-effect and photonic passivation are increasingly combined within single stacks.

Chemical passivation. Chemical passivation reduces the density of electronically active defects at surfaces and grain boundaries. In crystalline silicon, thin $Al_2O_3$ or $PO_x/Al_2O_3$ layers deposited by ALD or PECVD provide excellent chemical passivation of dangling bonds at both p-type and n-type surfaces, contributing to the first >20 % laboratory cells and now standard PERC rear stacks. In perovskites, small-molecule surface modifiers, halide-salt treatments, and 2D perovskite capping layers can fill halide vacancies, coordinate undercoordinated Pb and suppress non-radiative recombination, as shown for benzenamine-modified $MAPbI_3$ where synergistic passivation yields >21 % efficiency with improved moisture stability.

Field-effect passivation. Field-effect passivation uses fixed charges or dipoles in dielectric or interfacial layers to repel minority carriers from recombination-active interfaces. $Al_2O_3$ is the textbook example in c-Si: its negative fixed charge at the Si surface repels electrons at $p^+$-emitter surfaces, reducing surface recombination velocity when combined with adequate chemical passivation. In perovskite devices, LiF or other dipole-forming interlayers at the electron-selective contact introduce fixed charges and interfacial dipoles that enhance VOC via field-effect passivation, as demonstrated by Menzel and co-workers and in recent scalable $MAPbI_3$ and tandem architectures.

Photonic passivation. Photonic passivation refers to engineering the optical environment so that parasitic optical channels are suppressed while radiative recombination into useful modes is enhanced. Back reflectors based on *photonic crystals* or dielectric Bragg stacks can simultaneously act as excellent electrical passivation layers and as spectral/ angular reflectors that keep photons within the absorber, boosting both current and voltage. In thin-film Si and perovskite devices, such photonic-crystal back reflectors have been shown to increase long-wavelength EQE and JSC while also reducing rear-surface recombination through improved passivation and reduced parasitic absorption in the metal back contact.

These mechanisms are not independent: recent "full-scale" and "dual-field" passivation strategies explicitly combine surface reconstruction, chemical passivation and field-effect layers in wide-bandgap perovskites and perovskite/CIGS tandems, demonstrating that carefully designed stacks can simultaneously restrain ion migration, improve band alignment and maintain long-term stability.

**Table 7: Comparison of chemical, field-effect and photonic passivation**

| Passivation type | Physical principle | Typical implementations | Main benefits | Representative systems |
|---|---|---|---|---|
| Chemical | Reduce defect density (Dit, grain boundaries) | $Al_2O_3$, $PO_x/Al_2O_3$, SAMs, small molecules, salts | Lower SRH recombination, higher lifetime/VOC | c-Si, perovskites, CIGS, CdTe |
| Field-effect | Fixed charge/dipole repels minority carriers | $Al_2O_3$, $SiN_x$ stacks; LiF, ionic interlayers | Reduced surface recombination without heavy doping | c-Si emitters, perovskite ETL/HTL interfaces |
| Photonic | Shape LDOS and optical path (light trapping) | Photonic-crystal back reflectors, DBRs, metasurfaces | Enhanced EQE, photon recycling, lower optical loss | Thin-film Si, perovskite, tandems |

### 8.3. Integrating Laser Steps into Manufacturing Lines: Roll-to-Roll, Inline Metrology, and Yield

Scaling from laboratory cells to metre-scale modules requires that laser processing—P1/P2/P3 scribing, local annealing, defect repair—be tightly integrated into continuous production lines without sacrificing yield. For thin-film CdTe, CIGS, OPV and perovskites, laser patterning has become the *de facto* standard for monolithic series interconnection, because it is non-contact, maskless and compatible with both sheet-to-sheet and R2R webs.

In R2R perovskite manufacturing, slot-die coating, gas-knife drying, intermediate annealing and laser scribing must be carefully sequenced to avoid mechanical tension issues and local overheating. Recent demonstrations of fully R2R-processed perovskite cells and roll-to-sheet slot-die systems highlight the importance of synchronizing web speed, drying profiles and laser dwell times, enabling "ink-in, module-out" lines that can, in principle, run continuously.

To maintain high yield under such conditions, inline metrology is essential. Photoluminescence (PL) and electroluminescence (EL) imaging have emerged as powerful, contactless tools to monitor layer quality, detect shunts and quantify local recombination during or immediately after processing. Industrially oriented PL imaging setups now correlate spatial PL intensity and lifetime maps with IV parameters across multi-cell CIGS and perovskite modules, using automated Python-based data analysis pipelines. Such systems can flag defective regions arising from misaligned laser scribes, incomplete ablation, or local film defects, triggering real-time process corrections.

Laser processing itself can be coupled with in situ electrical measurements. Markauskas and co-workers, for example, used a direct electrical monitoring technique during P2/P3 scribing to optimize pulse duration, repetition rate and fluence, showing that properly tuned laser conditions minimize interconnect resistance and dead area while avoiding substrate damage. In perovskite lines, similar approaches combine fast IV/EL checks after each major step (e.g., perovskite deposition, transport-layer deposition, final laser scribing) to confine yield losses to early stages where rework is cheaper.

Looking forward, closed-loop process control that couples inline optical metrology (PL, EL, reflectance, scatterometry) with adaptive laser processing (dynamic fluence, spot size, and patterning strategy) is likely to be central to industrializing perovskite and tandem modules. R2R-oriented reviews emphasise that the combination of low-temperature deposition, sophisticated passivation stacks and integrated laser/inspection steps is key to unlocking low-cost, high-throughput and high-yield manufacturing at GW scale.

## 9. Opto-Electronic Modeling and Inverse Design for Light–Matter Engineered PV

### 9.1 Coupled Optical–Electrical Simulation: Transfer-Matrix, FDTD, and Drift– Diffusion Frameworks

Light–matter engineered photovoltaics (PV) including textured interfaces, nanophotonic scatterers, metasurface electrodes, and photon-recycling stacks are fundamentally governed by two coupled maps: (1) Maxwell's equations determine the position- and wavelength-dependent optical fields and absorption, and (2) that absorption sets the carrier-generation profile that drives transport, recombination, and the resulting J–V characteristics in the device (Deceglie, Ferry, Alivisatos, & Atwater, 2012). In practice, opto-electronic simulation computes a spatially resolved generation $G(r)(G(z)in\ 1d)$ from the optical solution and injects it as the source term in the semiconductor continuity equations, enabling nanostructure optimization while explicitly guarding against "optical wins" that inadvertently increase parasitic absorption in lossy layers or shift absorption into regions with poor collection (Deceglie *et al*., 2012). For laterally uniform multilayer stacks, the transfer-matrix method (TMM) provides a fast and interpretable route to optics: by enforcing electromagnetic boundary conditions at each interface, TMM yields reflectance/transmittance and the layer-resolved field intensity |E(z, λ)|²from which absorption in layer iii can be written in the common form $A_{\mathrm{i}}(\lambda) \propto \int_{z\in i} \alpha_{\mathrm{i}}(\lambda)|E(z,\lambda)|^2$ dz_and then converted into a generation profile via spectral integration (Yeh, 1988). Because TMM $A_{\mathrm{i}}(\lambda) \propto \int_{z\in i} \alpha_{\mathrm{i}}(\lambda)|E(z,\lambda)|^2$ dz is computationally inexpensive, it is routinely paired with 1D drift–diffusion device solvers for rapid sweeps over thickness, interference conditions, and angle/spectrum—an approach used explicitly in combined optical–electrical perovskite modeling pipelines (Bendib, Bencherif, Abdi, Meddour, Dehimi, & Chahdi, 2020). When the architecture is genuinely nanophotonic (gratings, nanopores, photonic crystals, plasmonic elements, nanoimprinted electrodes), full-wave field solvers such as finite-difference time-domain (FDTD) are typically required to capture diffraction, guided-mode resonances, strong near-fields, and absorption hot spots, including parasitic loss in metals or TCOs (Taflove & Hagness, 2005; Yee, 1966). In FDTD, the Yee-grid discretization advances Maxwell's equations in time under stability constraints and absorbing boundaries (e.g., PML), and the absorbed power density pabsp_abs(r, λ)is converted to carrier generation through $G(r) = \int p_a\, bs(r,\lambda)/(hc/\lambda)d\lambda$ within the active absorber (Taflove & Hagness, 2005). The electrical response is then modeled with drift–diffusion (DD), typically solving Poisson's equation coupled to electron and hole continuity equations with drift–diffusion currents and recombination terms (SRH, radiative, and Auger as appropriate), producing J–V curves, internal quantum efficiency trends, and loss attribution under realistic contacts and doping (Ren, Wang, Sha, & Choy, 2017; Selberherr, 1984). Numerically, the Scharfetter–Gummel discretization remains a widely used stable scheme for high-field junction transport (Scharfetter & Gummel, 1969). Finally, "coupled" modeling often needs to go beyond a one-way handoff of G(r) carrier-density-dependent optical effects (e.g., free-carrier absorption or index changes) can matter in some active media, and optics can also modify recombination physics through photon recycling, which changes the effective radiative saturation current and can boost Vo and performance as devices approach radiative limits (Brenes *et al*., 2019; Kirchartz *et al*., 2016; Wu *et al*., 2021).

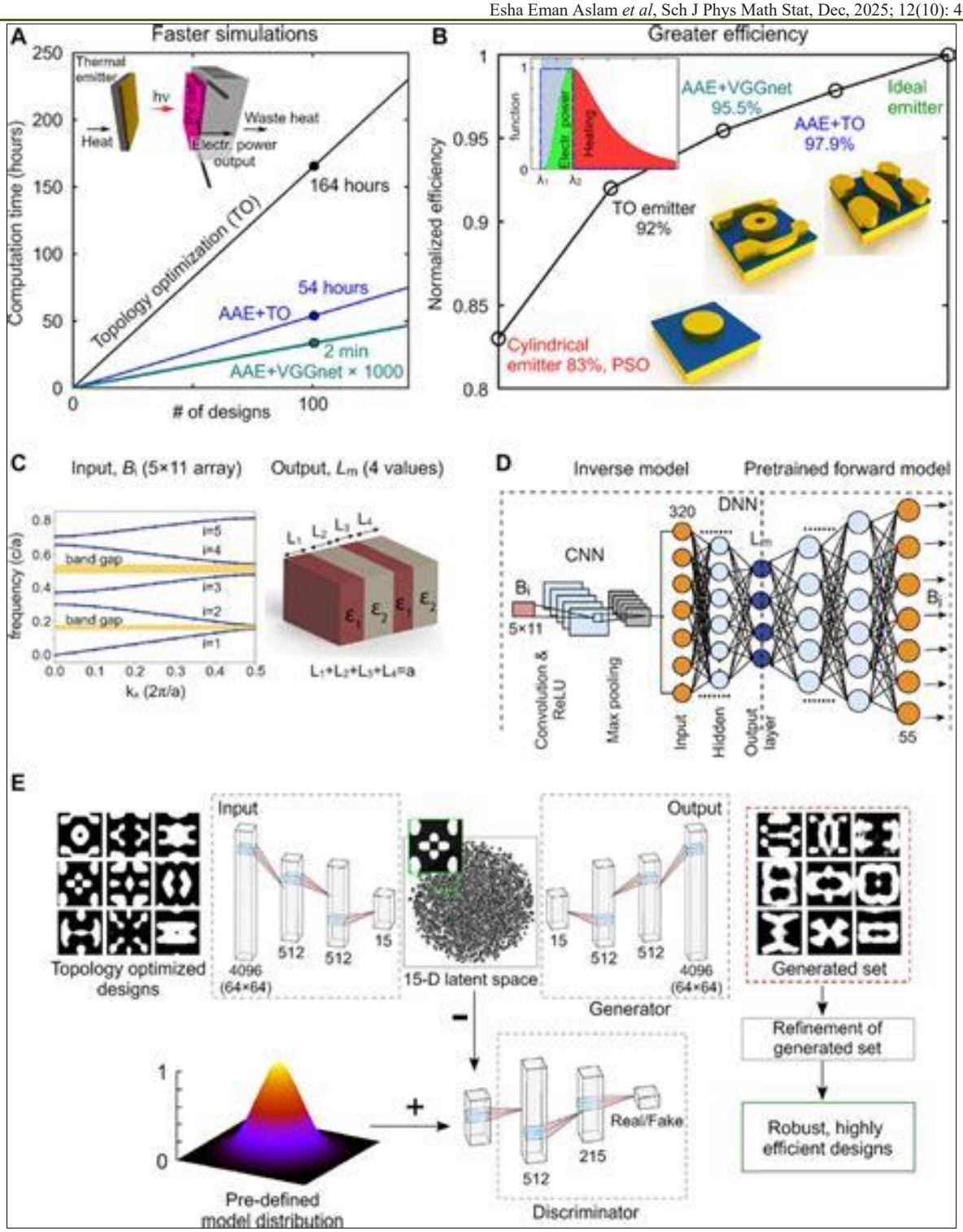


**Figure 5: FDTD-based *absorption enhancement* in a photonic-crystal-assisted perovskite solar cell**

FDTD-based absorption enhancement in a photonic-crystal-assisted perovskite solar cell means using finite-difference time-domain (FDTD) simulations to calculate how a photonic crystal structure (periodic nanostructure) changes the electric-field distribution in a perovskite solar cell. The photonic crystal can trap and scatter light, increase the optical path length, and create resonant modes, which leads to higher absorption in the perovskite layer and potentially a higher photocurrent.

### 9.2 Bridging Ultrafast Observables to Steady-State Performance and Inverse Design Strategies

Ultrafast experiments probe carrier physics on femtosecond–nanosecond timescales (thermalization, trapping, hot-carrier cooling, and early recombination), whereas PV performance is ultimately judged under millisecond-to-steady-state operation where quasi-Fermi level splitting, drift–diffusion transport to contacts, interfacial recombination, and resistive losses determine Voc, fill factor, and efficiency. The central multiscale

challenge is to convert what ultrafast (often contactless) measurements *directly* observe into device-ready parameters that remain physically consistent when used in steady-state device solvers (Li *et al*., 2020). In practice, transient absorption is commonly interpreted in terms of population decay channels (e.g., trapping, bimolecular and Auger recombination) and spectral signatures linked to band-edge and carrier-temperature effects; time-resolved photoluminescence separates radiative versus nonradiative contributions and constrains injection-dependent recombination; and THz/microwave photoconductivity provides early-time mobility/scattering information and (with decay dynamics) mobility–lifetime–type figures of merit. A notable community "predictive" approach explicitly combines contactless THz/microwave metrics with drift–diffusion modeling to anticipate current–voltage trends, offering a structured bridge from ultrafast observables to expected device behavior (Hempel *et al*., 2022).

A practical "translation layer" typically proceeds by fitting ultrafast kinetics with a minimal but physically grounded rate model (free carriers + traps + radiative channel, adding Auger if needed) to extract effective rate constants and injection-dependent lifetimes; these are then mapped into the coefficients used by steady-state drift–diffusion (DD) solvers effective SRH lifetimes (or trap parameters), radiative BBB, Auger CCC, and mobility $\mu$ followed by validation under device-relevant boundary conditions such as selective contacts, built-in fields, and interfacial recombination velocities (Li *et al*., 2020; Ren *et al*., 2017). Because a single simulation spanning femtoseconds to seconds is numerically stiff, multiscale PV modeling usually uses time-scale separation: an ultrafast block to determine early-time relaxation/trapping and generate effective initial conditions and rate coefficients, an intermediate block for diffusion/field-assisted separation and interfacial transfer (sometimes reduced-rate or kinetic approaches), and a device block where DD produces steady-state J–V and loss partitioning. This "stitching" becomes especially useful when early-time mobility/lifetime constraints are propagated into diffusion lengths and recombination currents that ultimately set Voc and fill factor in the steady-state regime (Hempel *et al*., 2022).

Machine-learning (ML) and inverse design become compelling in light–matter engineered PV because brute-force electromagnetic + DD co-optimization becomes expensive as design degrees of freedom grow (pixel/voxel geometries, multi-material stacks, broadband/angle constraints, and tolerance requirements). ML surrogates can learn fast forward mappings from structure to spectrum/fields, while inverse models attempt to map a target response back to candidate structures; because inverse problems are often ill-posed (many designs can yield similar responses), modern workflows frequently stabilize inverse design through constraints, tandem training (inverse + forward consistency), or by sampling multiple solutions with generative models (Liu *et al*., 2021; Moon *et al*., 2023). In parallel, adjoint and topology-optimization methods provide reliable gradient information for local improvement in high-dimensional photonic design spaces, and hybrid schemes combine gradient-based search with ML (for initialization, feasibility priors, or accelerated evaluation) to reduce the number of expensive full simulations (Christiansen & Sigmund, 2021; Deng *et al*., 2022; Molesky *et al*., 2018). For PV, the key point is that the objective is rarely "maximize absorption" alone: PV-real inverse design typically targets metrics such as maximizing Jsc while constraining parasitic absorption in metals/TCOs, improving Voc via reduced nonradiative recombination and/or photon-recycling-friendly photonics, and optimizing weighted efficiency under angular spectra, fabrication tolerances, and electrical constraints like collection probability and series resistance hence the need for opto-electronic co-optimization (Molesky *et al*., 2018; Ren *et al*., 2017).

### *10. Bridging Ultrafast Observables to Steady-State Performance and Machine-Learning Inverse Design in Light–Matter Engineered PV*

Ultrafast experiments probe photovoltaic (PV) materials on femtosecond–nanosecond timescales where carrier thermalization, trapping, hot-carrier cooling, and early recombination occur, while device performance is ultimately determined under millisecond-to-steady-state operation where quasi-Fermi level splitting, carrier transport to contacts, interfacial recombination, and resistive losses govern Voc, fill factor, and efficiency (Li *et al*., 2020). The key multiscale modeling challenge is to translate ultrafast observables into device-ready parameters without losing the underlying physics, so that spectroscopic signatures can be propagated into steady-state J–V behavior in a consistent way (Hempel *et al*., 2022).

Different ultrafast and contactless probes constrain different parts of the recombination–transport landscape. Transient absorption can resolve multi-component population dynamics and spectral signatures linked to trapping/detrapping, bimolecular and Auger recombination, state filling, and carrier-temperature/band-edge effects; time-resolved photoluminescence helps separate radiative versus nonradiative channels and constrain injection-dependent quasi-Fermi level splitting; and THz/microwave photoconductivity connects early-time photoconductivity to mobility and scattering while its decay reveals how mobility and lifetime evolve together as traps and recombination pathways become active (Li *et al*., 2020). A practical and increasingly adopted approach is to combine these contactless mobility/lifetime-type metrics with device-level modeling to predict current–voltage trends and screen materials in a way that better reflects operating

conditions than any single ultrafast metric alone (Hempel *et al*., 2022).

A robust "translation layer" typically begins by fitting ultrafast kinetics with a minimal, physically grounded rate model (free carriers + traps + radiative channel, adding Auger when high-injection behavior demands it) to extract effective rate constants and injection-dependent lifetimes. These outputs are then mapped into steady-state drift–diffusion inputs effective SRH lifetimes or trap parameters, radiative coefficient BBB, Auger coefficient C, and mobility μ\muwhich together set diffusion lengths, recombination currents, and quasi-Fermi level splitting under illumination (Li *et al*., 2020; Hempel *et al*., 2022). Because a single simulation spanning femtoseconds to seconds is numerically stiff, multiscale PV modeling commonly relies on time-scale separation: an ultrafast block supplies initial conditions and effective recombination/trapping rates, intermediate modeling captures diffusion/field-assisted separation and interfacial transfer when needed, and a device block uses drift–diffusion with realistic contacts and series resistance to produce steady-state J–V curves and loss attribution (Hempel *et al*., 2022).

Machine-learning (ML) and inverse design are especially valuable when light–matter engineered PV introduces large design spaces (textures, resonant photonic structures, metasurfaces, multilayer optical stacks) where brute-force electromagnetic simulation plus device-level optimization becomes computationally expensive (Molesky *et al*., 2018). Common paradigms include surrogate forward models that learn structure rightarrow spectrum/field responses to accelerate evaluation, inverse models that learn target response right candidate structures (often requiring regularization because the inverse problem is non-unique), and generative approaches that propose multiple diverse designs consistent with a target so that manufacturability and robustness constraints can be applied downstream (Liu *et al*., 2021; Ma *et al*., 2022; Molesky *et al*., 2018). In parallel, adjoint and topology-optimization methods remain a backbone for high-dimensional photonic inverse design because they compute sensitivities to many degrees of freedom efficiently and can be extended to enforce discreteness and fabrication constraints (Christiansen & Sigmund, 2021; Molesky *et al*., 2018). For PV, the objective is rarely "maximize absorption" alone; instead, device-real inverse design targets metrics like maximizing Jsc while limiting parasitic absorption in metals/TCOs, improving Voc by suppressing nonradiative recombination and enabling photon-recycling-friendly optics, and optimizing performance under angular spectra, tolerances, and electrical constraints such as collection probability, contact selectivity, and series resistance—so the most reliable workflows incorporate opto-electronic (not optical-only) objectives, either through coupled solvers or electrical-response surrogates (Liu *et al*., 2021; Molesky *et al*., 2018).

## REFERENCES


- Abbas, M., Xu, X., Rauf, M., & Kyaw, A. K. K. (2024). A comprehensive review on defects-induced voltage losses and strategies toward highly efficient and stable perovskite solar cells. *Photonics, 11*, 87.
- Ahmad, N. I., *et al*. (2023). A comprehensive review of flexible cadmium telluride solar cells. *Nanomaterials, 13*, 3520.
- Alanazi, T. I., *et al*. (2023). Current spray-coating approaches to manufacture perovskite solar cells. Sustainable Energy & Fuels, 7, 6206–6233.
- Albaladejo-Siguan, M., *et al*. (2021). Stability of quantum dot solar cells: A matter of lifetime. *Advanced Energy Materials, 11*, 2103457.
- Ali Ahmad, S. O., *et al*. (2021). Application of two-dimensional materials in perovskite solar cells. *Journal of Renewable and Sustainable Energy, 13*, 043501.
- Allen, T. G., Bullock, J., Yang, X., Javey, A., & De Wolf, S. (2019). Passivating contacts for crystalline silicon solar cells. Nature Energy, 4(11), 914–928.
- Amalathas, A. P., & Alkaisi, M. M. (2019). Nanostructures for light trapping in thin film solar cells. Micromachines, 10(9), 619.
- Asanov, N., *et al*. (2024). Optical and photovoltaic properties of organic solar cells: A comprehensive modeling study. *Physical Review B, 109*, 205201.
- Ashrafi-Peyman, Z., *et al*. (2024). An elliptical nanoantenna array plasmonic metasurface for solar absorption enhancement. Nanoscale Research Letters, 19, 1–12.
- Baiju, A., *et al*. (2022). Status and challenges of multijunction solar cell technology. *Semiconductors, 56*, 1005-1030.
- Balachninaitė, O., *et al*. (2025). Influence of unidirectional polishing on the formation of laser-induced periodic surface structures on steel. Scientific Reports, 15, 19844.
- Baloch, A. A. B., Ahmed, I., Noman, M., & Yong, C. K. (2018). Practical efficiency limit of methylammonium lead iodide perovskite solar cells. The Journal of Physical Chemistry Letters, 9, 4263–4270.
- Banik, S., *et al*. (2025). Femtosecond laser-induced surface structuring for enhanced light trapping. Solar Energy Materials and Solar Cells, 267, 112345.
- Basumatary, P. (2022). A short review on progress in perovskite solar cells. *Materials Research Bulletin, 154*, 111884.
- Baumann, S., Hanisch, J., Kroyer, T., Driver, M., Zhang, H., Kauffmann, Y., & Tress, W. (2023). Stability and reliability of perovskite containing solar cells. *Solar Energy Materials and Solar Cells, 243*, 112164.

- Bendib, T., Bencherif, H., Abdi, M. A., Meddour, F., Dehimi, L., & Chahdi, M. (2020). Combined optical–electrical modeling of perovskite solar cell with an optimized design. *Optical Materials, 109*, 110259.
- Bishop, J. E., *et al*. (2020). Development of spray-coated perovskite solar cells. Advanced Energy Materials, 10, 1903213.
- Black, L. E., Meyer, A. R., Wilshaw, P. R., & Hall, S. (2018). $POx/Al_2O_3$ stacks: Highly effective surface passivation of crystalline silicon. Applied Physics Letters, 112(20), 201603.
- Bowman, A. R., *et al*. (2020). Quantifying photon recycling in solar cells and light-emitting diodes. Journal of Applied Physics, 127(8), 083103.
- Bowman, A. R., Savill, K. J., Patel, J. B., Snaith, H. J., & Senanayak, S. P. (2022). Extracting decay rate ratios from photoluminescence quantum efficiency and lifetime measurements in halide perovskites. Journal of Applied Physics, 131, 153102.
- Brenes, R., Laitz, M., Jean, J., deQuilettes, D. W., & Bulović, V. (2019). Benefit from photon recycling at the maximum-power point of a solar cell. *Physical Review Applied, 12*(1), 014017.
- Brenes, R., Laitz, M., Jean, J., deQuilettes, D. W., & Bulović, V. (2019). Benefit from photon recycling at the maximum-power point of state-of-the-art perovskite solar cells. Physical Review Applied, 12(1), 014017.
- Brongersma, M. L., Cui, Y., & Fan, S. (2014). Light management for photovoltaics using high-index nanostructures. Nature Materials, 13(5), 451–460.
- Bullock, J., Hettick, M., Geissbühler, J., Ong, A. J., Allen, T., Sutter-Fella, C. M., Yan, D., Zhang, X., De Wolf, S., Cuevas, A., Ballif, C., & Javey, A. (2016). Efficient silicon solar cells with dopant-free asymmetric heterocontacts. Nature Energy, 1, 15031.
- Bullock, J., Wan, Y., Xu, Z., Essig, S., Hettick, M., Wang, H., Ji, W., Boccard, M., Cuevas, A., Ballif, C., & Javey, A. (2018). Stable dopant-free asymmetric heterocontact silicon solar cells with efficiencies above 20%. ACS Energy Letters, 3(3), 508–513.
- Burkitt, D., *et al*. (2020). Roll-to-roll slot-die coated p–i–n perovskite solar cells. Sustainable Energy & Fuels, 4, 2844–2855.
- Carlson, D. E. (2012). Laser processing of solar cells. Proceedings of SPIE, 8473, 847302.
- Casalini, S., Bortolotti, C. A., Leonardi, F., & Biscarini, F. (2017). Self-assembled monolayers in organic electronics. Chemical Society Reviews, 46(1), 40–71.
- Chandrasekhar, P. S., *et al*. (2022). Rapid scalable fabrication of roll-to-roll slot-die coated perovskite solar cells. Sustainable Energy & Fuels, 6, 2860–2872.
- Chang, Y. C., *et al*. (2022). Investigation of the laser doping and plating process for cost-effective highly efficient silicon solar cells. Solar Energy Materials and Solar Cells, 236, 111527.
- Chen, H., Cao, Q., Pu, X., Zhao, Q., He, X., Zhou, Z., Tajibaev, I., Boynazarov, I., Bai, Y., Jia, S., & Li, X. (2025). Strong coupling of NiOx and self-assembled molecules via inserted reductant for high-performance inverted perovskite solar cells. Advanced Materials, 37(43), e10553.
- Chen, X., *et al*. (2024). Surface engineering for enhanced efficiency and stability of perovskite solar cells. *Materials Today Physics, 40*, 101332.
- Chen, X., Li, Y., Zhu, H., & Fang, H. (2024). Charge transfer kinetics in halide perovskites. ACS Energy Letters, 9, 1234–1256.
- Cho, A. J., *et al*. (2018). Two-dimensional $WSe_2/MoS_2$ p–n heterojunction-based transparent photovoltaic cell and its performance enhancement by fluoropolymer passivation. *ACS Applied Materials & Interfaces, 10*, 38967–38975.
- Cho, C., *et al*. (2021). Effects of photon recycling and scattering in high-performance perovskite solar cells. Advanced Energy Materials, 11(2), 2003380.
- Christiansen, R. E., & Sigmund, O. (2021). Inverse design in photonics by topology optimization: Tutorial. *Journal of the Optical Society of America B, 38*(2), 496–509.
- Chu, Z., *et al*. (2025). Laser annealing enables rapid, degradation-free ambient processing of perovskite solar modules. Science, 387(6655), 45–51.
- Cinquanta, E., Sato, S. A., Kauch, A., *et al*. (2019). Ultrafast THz probe of photoinduced polarons in lead-halide perovskites. Physical Review Letters, 122, 166601.
- Cordell, J. J., *et al*. (2023). Technoeconomic analysis of perovskite silicon tandem solar modules. *Joule, 7*, 1–24.
- Cordell, J. J., *et al*. (2025). Technoeconomic analysis of perovskite/silicon tandem modules. *Joule, 9*, 1–24.
- Deceglie, M. G., Ferry, V. E., Alivisatos, A. P., & Atwater, H. A. (2012). Design of nanostructured solar cells using coupled optical and electrical modeling. *Nano Letters, 12*(6), 2894–2900.
- deQuilettes, D. W., Burke, S., Ziffer, M. E., & Ginger, D. S. (2019). Charge-carrier recombination in hybrid halide perovskites. Accounts of Chemical Research, 52(2), 400–409.
- deQuilettes, D. W., Koch, S., Burke, S., Paranji, R. K., Shropshire, A. J., Ziffer, M. E., & Ginger, D. S. (2016). Photoluminescence lifetimes exceeding eight microseconds and quantum yields exceeding 30% in hybrid perovskite thin films by ligand passivation. ACS Energy Letters, 1(2), 438–444.
- deQuilettes, D. W., Laitz, M., Brenes, R., Dou, B., Snaith, H. J., & Ginger, D. S. (2020). Maximizing the external radiative efficiency of hybrid perovskite solar cells. Pure and Applied Chemistry, 92(5), 697–706.

- deQuilettes, D. W., Vorpahl, S. M., Stranks, S. D., Nagaoka, H., Eperon, G. E., Ziffer, M. E., & Ginger, D. S. (2015). Impact of microstructure on local carrier lifetime in perovskite solar cells. Science, 348(6235), 683–686.
- Ding, Y., *et al*. (2025). Two-dimensional type-II van der Waals heterostructure $MASnBr_3/MoS_2$ for tunable optoelectronic devices. *Applied Surface Science,*
- Doherty, T. A. S., Winchester, A. J., Macpherson, S., Johnstone, D. N., Pareek, V., Tennyson, E. M., Kosar, S., Richter, J. M., Labram, J. G., Davies, D. W., Frost, J. M., Walsh, A., Midgley, P. A., & Stranks, S. D. (2020). Performance-limiting nanoscale trap clusters at grain boundaries in halide perovskites. Nature Energy, 5(1), 69–77.
- Dostovalov, A., *et al*. (2020). Hierarchical anti-reflective laser-induced periodic surface structures on silicon. Nanoscale, 12(27), 14317–14326.
- Dou, B., *et al*. (2018). Roll-to-roll printing of perovskite solar cells. ACS Energy Letters, 3, 2558–2565.
- Duan, L., Walter, D., Chang, N., Bullock, J., Phang, S. P., & Shen, H. (2023). Stability challenges for the commercialization of perovskite silicon tandem solar cells. *Nature Reviews Materials, 8*, 261–281.
- Dunbar, R. B., *et al*. (2012). Highly absorbing solar cells—a survey of plasmonic nanostructures. Optics Express, 20(S2), A177–A189.
- Elhady, F., *et al*. (2021). A review of thin film solar cells. *Journal of Basic and Environmental Sciences, 8*, 36-46.
- Erwin, W. R., *et al*. (2016). Light trapping in mesoporous solar cells with plasmonic nanoparticles: A review. Energy & Environmental Science, 9(5), 1577–1601.
- Fan, W., *et al*. (2023). Influence of $Al_2O_3/SiN_x$ rear-side stacked passivation on crystalline silicon solar cells. Energies, 16, 6963.
- Fell, A., Niewelt, T., & Steinhauser, B. (2021). Radiative recombination in silicon photovoltaics: Modeling the influence of charge carrier densities and photon recycling. Solar Energy Materials and Solar Cells, 230, 111998.
- Fu, W., Soliman, A. I. A., Zheng, Y., Zhou, Y., Zhang, Y., Shan, S., & Chen, H. (2025). Self-assembled monolayers for perovskite solar cells. Review of Materials Research, 1(1), 100017.
- Garnett, E. C., Ehrler, B., Polman, A., & Alarcón Lladó, E. (2021). Photonics for photovoltaics: Advances and opportunities. *ACS Photonics, 8*, 61–70.
- Gatto, L., Mics, Z., Turchinovich, D., & Bonn, M. (2021). Time-resolved terahertz spectroscopy for probing the mobility and diffusion length in $CsPbBr_3$ nanocrystals. Journal of Physical Chemistry C, 125, 12345–12355.
- Geng, C., *et al*. (2024). Crystallization modulation and holistic passivation for monolithic perovskite/CIGS tandems. Advanced Energy Materials, 14, 2401221.
- Gong, J., Xu, L., Chen, W., & Li, X. (2023). Ultrafast dynamics in perovskite based optoelectronic devices. *Advanced Materials, 35*, 2208741.
- Green, M. A., Dunlop, E. D., Hohl Ebinger, J., Yoshita, M., Kopidakis, N., & Hao, X. (2023). Solar cell efficiency tables (version 62). *Progress in Photovoltaics: Research and Applications, 31*, 3–16.
- Green, M. A., Dunlop, E. D., Hohl-Ebinger, J., Yoshita, M., Kopidakis, N., & Hao, X. (2023). Solar cell efficiency tables (version 62). *Progress in Photovoltaics: Research and Applications, 31*, 3-16.
- Hall, R., *et al*. (2021). Back contacts materials used in thin film CdTe solar cells: A review. *Energy Science & Engineering, 9*, 1677-1703.
- Hempel, H., Savenije, T. J., Stolterfoht, M., Neu, J., Failla, M., Paingad, V. C., Kužel, P., Heilweil, E. J., Spies, J. A., Schleuning, M., & others. (2022). Predicting solar cell performance from terahertz and microwave spectroscopy. *Advanced Energy Materials, 12*(13), 2102776.
- Hempel, H., Stolterfoht, M., Caprioglio, P., *et al*. (2022). Predicting solar cell performance from terahertz and microwave spectroscopies. Advanced Energy Materials, 12, 2102776.
- Herz, L. M. (2016). Charge-carrier dynamics in organic–inorganic metal halide perovskites. Annual Review of Physical Chemistry, 67, 65–89.
- Herz, L. M. (2016). Charge-carrier dynamics in organic–inorganic metal halide perovskites. Annual Review of Physical Chemistry, 67, 65–89.
- Hodes, G. (2015). Understanding the implication of carrier diffusion length in halide perovskite solar cells. The Journal of Physical Chemistry Letters, 6, 4090–4092.
- Hoex, B., Schmidt, J., Bock, R., Altermatt, P. P., van de Sanden, M. C. M., & Kessels, W. M. M. (2008). Silicon surface passivation by atomic layer deposited $Al_2O_3$. Journal of Applied Physics, 104(4), 044903.
- Hsiao, Y.-S., *et al*. (2012). Improving the light trapping efficiency of plasmonic polymer solar cells through metallic nanoparticle distribution control. Journal of Physical Chemistry C, 116(35), 20731–20737.
- Hu, B., Li, J., Zhang, Y., & Tang, J. (2025). Revealing trapped carrier dynamics at buried interfaces in perovskite solar cells. Advanced Materials, 37, 2207160.
- Huang, J., Li, B., Wang, S., Shi, B., Zhao, Y., & Zhang, X. (2025). A review on perovskite silicon tandem solar cells. *Energies, 18*, 4327.
- Huang, K., *et al*. (2024). Laser processing of CdTe-based thin-film solar cells on flexible glass substrates. Solar Energy, 274, 112412.

- Iqbal, M. T., Saeeda, S., Zahra, T., Umar, Z., Khan, W. Z., Adnan, M., Raza, H., Shah, G. A., & Toffique, M. (2025). Next-generation materials discovery using density functional theory: Functional innovation, solar energy, catalysis, and eco toxicity modelling. Scholars Journal of Engineering and Technology, 13(7), 454–486. https://doi.org/10.36347/sjet.2025.v13i07.003
- Ishteev, R., *et al*. (2024). Technological parameters of thin-film pulsed laser scribing for photovoltaic applications. Clean Energy, 8(3), 127–140.
- Isikgor, F. H., Ramanujam, J., Khan, M. R., Gursoy, S., & Mathur, S. (2022). Molecular engineering of contact interfaces for high-performance perovskite solar cells. Nature Reviews Materials, 8, 89–108.
- Jamaatisomarin, F., Chen, R., Hosseini Zavareh, S., & Lei, S. (2023). Laser scribing of photovoltaic solar thin films: A review. *Journal of Manufacturing and Materials Processing, 7*, 94.
- Jariwala, S., Garnett, E. C., & Ehrler, B. (2019). Imaging grain structure in halide perovskite solar cells. Advanced Energy Materials, 9, 1902523.
- Johnston, M. B., & Herz, L. M. (2016). Hybrid perovskites for photovoltaics: Charge-carrier recombination, diffusion, and radiative efficiencies. Accounts of Chemical Research, 49, 146–154.
- Khadka, D. B., *et al*. (2024). Defect passivation in methylammonium-free perovskite solar cells using diammonium molecules. Nature Communications, 15, 45228.
- Khan, H. Z., *et al*. (2025). Advancements in metasurfaces for polarization control. Journal of Photonics and Optoelectronics, 7(1), 1–35.
- Khan, J. I., Lee, S. H., & Park, N. G. (2024). Evaluation of interfacial photophysical processes by time-resolved spectroscopy in perovskite solar cells. Matter, 7, 2150–2172.
- Khan, W. Z. (2024). Across the spectrum: Imaging and spectroscopy as the common thread of physics from quantum-scale probes to ultrafast & high-energy [ResearchGate publication page]. ResearchGate. Retrieved December 17, 2025
- Khan, W. Z. (2025). Advanced engineering of ZnO nanoparticles: Enhancing structural, magnetic, and optical properties via Co and Cu doping [ResearchGate publication page]. ResearchGate. Retrieved December 17, 2025
- Khan, W. Z. (2025). Advancing double perovskites: Tailoring optoelectronic, magnetic, and transport properties for sustainable energy and next-generation technologies [ResearchGate publication page]. ResearchGate. Retrieved December 17, 2025
- Khan, W. Z. (2025). An interdisciplinary review of modern computer science and IT: From cloud, IoT, and AI to quantum computing and cybersecurity [ResearchGate publication page]. ResearchGate. Retrieved December 17, 2025
- Khan, W. Z. (2025). DFT study of optoelectronic and thermoelectric properties of halide double perovskite $Rb_2TlSbX_6$ (X = Cl, Br, I) for solar cell applications [ResearchGate publication page]. ResearchGate. Retrieved December 17, 2025
- Khan, W. Z. (2025). Laser technology: Bridging historical milestones and modern applications in science, industry, and sustainability [ResearchGate publication page]. ResearchGate. Retrieved December 17, 2025
- Khan, W. Z. (2025). Multifunctional nanomaterials in materials chemistry: A cross-disciplinary review of applications in energy, environment, catalysis, and biomedicine [ResearchGate publication page]. ResearchGate. Retrieved December 17, 2025.
- Khan, W. Z. (2025). Nanotechnology for perovskite solar cells: Solving efficiency, stability and energy storage challenges [ResearchGate publication page]. ResearchGate. Retrieved December 17, 2025
- Khan, W. Z. (2025). Perovskite solar cell efficiency via tunable Ag nanoparticle-integrated $SnO_2$ transport layers: Mechanistic insights and air-fabrication approach [ResearchGate publication page]. ResearchGate. Retrieved December 17, 2025.
- Khan, W. Z. (2025). Role of spin-orbit coupling in Bi-rich to In-rich $Cs_2Ag(In_xBi_{1-x})Cl_6$ double perovskite structures: Electronic and optical design [ResearchGate publication page]. ResearchGate. Retrieved December 17, 2025
- Khan, W. Z. (2025). Synthesis and characterization of La-doped BNBT lead-free ceramics with enhanced piezoelectric and dielectric properties [ResearchGate publication page]. ResearchGate. Retrieved December 17, 2025
- Khan, W. Z. (2025). Theoretical design and optoelectronic analysis of lead-free $CsPbX_3/Cs_2SnX_6$ core-shell perovskite nanocrystals for enhanced stability and charge dynamics [ResearchGate publication page]. ResearchGate. Retrieved December 17, 2025
- Khan, W. Z. (2025). Unified intelligence: A comprehensive review of the development, applications, and future directions of AI, ML, deep learning, and data science in modern technology [ResearchGate publication page]. ResearchGate. Retrieved December 17, 2025
- Khan, W. Z., Javed, K., Shah, S. M. A., Umar, Z., Zahid, T., Parvaiz, M., & Asim, S. (2025). First demonstration of a photo-rechargeable lead-free $Cs_2NaBiI_6$ double perovskite: Toward sustainable integrated photobattery devices. Scholars Journal of Physics, Mathematics and Statistics, 12(8), 346–356.
- Khan, W. Z., Rehman, H. M. A., Ali, M. W., Nadeem, M. S., Asim, S., Mahmood, K., Qasim, M. I., Shah, S. M. W., Ali, T., & Shah, S. M. A. (2025). Cross-disciplinary research gaps and future challenges in physics, chemistry, material science, and medical fields: A comprehensive exploration. Scholars International Journal of Chemistry and

Material Sciences, 8(11), 364–419. https://doi.org/10.36347/sijcms.2025.v08i11.001

- Khan, W. Z., Umar, Z., Baloch, M. H., Saeeda, S., Ahmad, M. Y., Zahra, T., Mustafa, U., Khan, S., & Mahmood, R. N. (2025). AI-driven and quantum-informed design of functional nanomaterials: Revolutionizing materials discovery. Scholars Journal of Engineering and Technology, 13(10), 974–1012. https://doi.org/10.36347/sjet.2025.v13i10.002
- Kim, S. Y., Cho, S. J., Byeon, S. E., He, X., & Yoon, H. J. (2020). Self-assembled monolayers as interface engineering nanomaterials in perovskite solar cells. Advanced Energy Materials, 10(23), 2002606.
- Kirchartz, T., & Rau, U. (2018). Radiative recombination limits of solar cells with band gaps between 1 and 2 eV. Journal of Applied Physics, 123, 113101.
- Kirchartz, T., Markvart, T., Rau, U., & others. (2016). Impact of photon recycling on the open-circuit voltage of perovskite solar cells. *ACS Energy Letters*.
- Kovacic, M., *et al*. (2019). Light management design in ultra-thin chalcopyrite solar cells. *Solar Energy Materials and Solar Cells, 200*, 109933.
- Li, C., & colleagues. (2020). Insights into ultrafast carrier dynamics in perovskite thin films and solar cells. *ACS Photonics, 7*(8), 1893–1907.
- Li, C., Guerrero, A., Huettner, S., & Bisquert, J. (2020). Insights into ultrafast carrier dynamics in perovskite thin films and solar cells. *ACS Photonics, 7*, 8–18.
- Li, H., *et al*. (2022). Fully roll-to-roll processed efficient perovskite solar cells. Nano Research, 15, 7443–7454.
- Li, J., *et al*. (2021). A brief review of high efficiency III-V solar cells for space applications. *Frontiers in Physics, 8*, 631925.
- Lin, H., Yang, M., Ru, X., Wang, G., Yin, S., Peng, F., Hong, C., Qu, M., Lu, J., Fang, L., Han, C., Isabella, O., Gao, P., & Li, Z. (2023). Silicon heterojunction solar cells with electrically optimized nanocrystalline-silicon hole contact layers. Nature Energy, 8(8), 789–799.
- Liu, S., Li, C., Zhang, Y., Wang, X., Chen, W., Chen, R., Zhao, L., Chen, Q., & Zhou, H. (2024). Buried interface molecular hybrid for inverted perovskite solar cells. Nature, 632, 536–542.
- Liu, Z., Zhu, D., Raju, L., & Cai, W. (2021). Tackling photonic inverse design with machine learning. *Advanced Science, 8*(5), 2002923.
- Ma, T., Tobah, M., Wang, H., & Guo, L. J. (2022). Benchmarking deep learning-based models on nanophotonic inverse design problems. *Opto-Electronic Science, 1*, 210012.
- Maier, S. A. (2007). Plasmonics: Fundamentals and applications. Springer.
- Marques, A. S., *et al*. (2021). Low-temperature blade-coated perovskite solar cells. Industrial & Engineering Chemistry Research, 60, 9299–9308.
- Mascaretti, L., Chen, Y., Henrotte, O., Yesilyurt, O., & co-authors. (2023). Designing metasurfaces for efficient solar energy conversion. ACS Photonics, 10(12), 4079–4103.
- Menzel, D., *et al*. (2022). Field-effect passivation in perovskite solar cells by a LiF interlayer. Advanced Energy Materials, 12, 2201109.
- Molesky, S., Lin, Z., Piggott, A. Y., Jin, W., Vučković, J., & Rodriguez, A. W. (2018). Inverse design in nanophotonics. *Nature Photonics, 12*(11), 659–670.
- Molpeceres, C., *et al*. (2012). Parameterization of local laser doping and laser-fired contacts for silicon solar cells. Physics Procedia, 39, 670–678.
- Monti, M. (2020). Ultrafast spectroscopy of metal halide perovskites and III–V nanostructures (Doctoral dissertation, University of Warwick).
- Muñoz García, C., *et al*. (2022). Influence of wavelength and pulse duration on the laser scribing of transition metal oxides for crystalline silicon solar cells. Applied Surface Science, 590, 153115.
- Nakamura, T., Imaizumi, M., Akiyama, H., & Okada, Y. (2020). Practical target values of Shockley–Read–Hall recombination rates in state-of-the-art triple-junction solar cells for realizing conversion efficiencies within 1% of the internal radiative limit. Progress in Photovoltaics: Research and Applications, 28, 1157–1167.
- Nanosecond Laser Scribing of CIGS Thin Film Solar Cells. (2018). Applied Physics Letters, 112(13), 134102.
- Niewelt, T., Steinmetz, L., Hagendorf, C., & Murphy, J. D. (2022). Reassessment of intrinsic bulk recombination in crystalline silicon. Solar Energy Materials and Solar Cells, 234, 111441.
- Ning, W., Tetzlaff, D., & Damjanovic, V. (2018). Long electron–hole diffusion length in high-quality lead halide perovskite single crystals. The Journal of Physical Chemistry Letters, 9, 2066–2073.
- Ochoa, M., Li, Z., Márquez, J., *et al*. (2022). Charge carrier lifetime fluctuations and performance in polycrystalline thin-film solar absorbers revealed by time-resolved photoluminescence microscopy. Advanced Energy Materials, 12, 2102800.
- Oliveira, A. J. N., *et al*. (2022). Exploiting the optical limits of thin-film solar cells: A review on advanced light management. *Advanced Photonics Research, 3*, 2100190.
- Palma, A. L. (2020). Laser processed perovskite solar cells and modules. *Solar RRL, 4*, 1900432.
- Parvazian, E., *et al*. (2024). The roll-to-roll revolution to tackle the industrial leap for perovskite photovoltaics. Nature Communications, 15, 48518.
- Peters, J. A., Unger, E. L., & Savenije, T. J. (2019). Carrier recombination in $MAPbI_3$ revealed by time-

resolved photoluminescence spectroscopy. Physical Review B, 100, 235305.

- Ponseca, C. S., Jr., Savenije, T. J., Abdellah, M., *et al*. (2016). Revealing the ultrafast charge carrier dynamics in organometal halide perovskites using time-resolved terahertz spectroscopy. Nanoscale, 8, 6278–6284.
- Qiu, X., Domanski, K., & Stranks, S. D. (2023). Probing charge carrier dynamics in perovskite solar cells. *Chemical Reviews, 123*, 2872–2920.
- Raisa, A. T., *et al*. (2025). Advances in multijunction solar cells: An overview. *Materials Today Energy, 35*, 101434.
- Raja, W., De Bastiani, M., Allen, T. G., Aydin, E., & co-authors. (2021). Photon recycling in perovskite solar cells and its impact on device design. Nanophotonics, 10(8), 1961–1983.
- Rau, U. (2014). Thermodynamics of light management in photovoltaic devices. Physical Review B, 90(3), 035211.
- Rebegea, S. A. (2018). Nanosecond laser ablation of thin film material libraries (Doctoral dissertation, University of Birmingham).
- Ren, X., Wang, Z., Sha, W. E. I., & Choy, W. C. H. (2017). Exploring the way to approach the efficiency limit of perovskite solar cells by drift–diffusion model. *ACS Photonics, 4*(4), 934–942. Scharfetter, D. L., & Gummel, H. K. (1969). Large-signal analysis of a silicon Read diode oscillator. *IEEE Transactions on Electron Devices, 16*(1), 64–77.
- Review of Laser Doping and its Applications in Silicon Solar Cells. (2025). Progress in Photovoltaics: Research and Applications, 33(4), 321–345.
- Richter, A., Glunz, S. W., Werner, F., Schmidt, J., & Cuevas, A. (2012). Improved quantitative description of Auger recombination in crystalline silicon. Physical Review B, 86, 165202.
- Riley, D. B., Meredith, P., & Armin, A. (2024). Exciton diffusion in organic semiconductors: Precision and pitfalls. Nanoscale, 16, 1234–1254.
- Robust Estimation of Charge Carrier Diffusivity. (2022). Robust estimation of charge carrier diffusivity using transient photoluminescence microscopy. The Journal of Chemical Physics, 157, 104201.
- Romeo, A., *et al*. (2021). CdTe-based thin film solar cells: Past, present and future. *Energies, 14*, 1684.
- Saive, R. (2021). Light trapping in thin silicon solar cells: A review on fundamentals and technologies. *Progress in Photovoltaics: Research and Applications, 29*, 1125–1149.
- Saive, R. (2021). Light trapping in thin silicon solar cells: A review on fundamentals and technologies. *Progress in Photovoltaics: Research and Applications, 29*, 1125-1149.
- Schmidt, J., Kerr, M., Bothe, K., & Cuevas, A. (2012). Advances in the surface passivation of silicon solar cells. Energy Procedia, 27, 361–372.
- Schmidt, J., Veith, B., Bock, R., & Altermatt, P. P. (2008). Effective surface passivation of crystalline silicon using ultrathin $Al_2O_3$ films and $Al_2O_3/SiN_x$ stacks. Progress in Photovoltaics: Research and Applications, 16(6), 461–466.
- Selberherr, S. (1984). *Analysis and simulation of semiconductor devices*. Springer. Taflove, A., & Hagness, S. C. (2005). *Computational electrodynamics: The finite-difference time-domain method* (3rd ed.). Artech House.
- Shen, T., Zhang, H., & Liu, Y. (2022). Time-resolved spectroscopy for the study of perovskite optoelectronic devices. Chinese Journal of Electronics, 31, 1152–1164.
- Shin Thant, K. K., *et al*. (2025). Comprehensive review on slot-die-based perovskite solar cells. Advanced Energy Materials, 15, 2403088.
- Shockley, W., & Queisser, H. J. (1961). Detailed balance limit of efficiency of p–n junction solar cells. *Journal of Applied Physics, 32*, 510–519.
- Shockley, W., & Read, W. T. (1952). Statistics of the recombination of holes and electrons. Physical Review, 87(5), 835–842.
- Shockley, W., & Read, W. T. (1952). Statistics of the recombination of holes and electrons. Physical Review, 87, 835–842.
- Sizov, D., Rodionov, I., & Goodilin, E. (2019). Self-assembled interface monolayers for organic and hybrid electronics. Russian Chemical Reviews, 88(10), 993–1037.
- Soderström, K., *et al*. (2013). Coupling light into thin silicon layers for high-efficiency solar cells. In *Thin Film Solar Cells* (pp. 205-242).
- Song, C., *et al*. (2025). Laser processing in halide photovoltaic cells. Bioengineering & Translational Medicine, 10(1), e20240010.
- Soufiani, A. M., *et al*. (2016). Electro- and photoluminescence imaging as fast screening tools for perovskite solar cells. Journal of Applied Physics, 120, 035702.
- Soufiani, A. M., Huang, F., Reece, P., Xia, H., & Ho-Baillie, A. (2015). Polaronic exciton binding energy in iodide and bromide organic–inorganic lead halide perovskites. Applied Physics Letters, 107, 231902.
- Srivastava, S., Cho, H., & Park, N. G. (2023). Advanced spectroscopic techniques for characterizing defects and interfaces in halide perovskites. Communications Materials, 4, 49.
- Starczewska, A., *et al*. (2024). Photonic crystal structures for photovoltaic applications. Nanomaterials, 14, 813.
- Staub, F., Monahan, N. R., Rieder, M., Wu, X., Trinh, M. T., Zhu, X. Y., & Bonn, M. (2018). Statistics of the Auger recombination of electrons

and holes via defect levels in the band gap: Application to lead-halide perovskites. ACS Omega, 3, 8994–9005.

- Stranks, S. D., & Snaith, H. J. (2015). Metal-halide perovskites for photovoltaic and light-emitting devices. Nature Nanotechnology, 10(5), 391–402.
- Sugie, A., Nakano, K., Tajima, K., Osaka, I., & Yoshida, H. (2023). Dependence of exciton binding energy on bandgap of organic semiconductors. The Journal of Physical Chemistry Letters, 14, 11412–11420.
- Sun, D., *et al*. (2023). Enhanced performance in perovskite films by defect passivation via pulsed laser annealing and $MoS_2$ doping. Nano Energy, 104, 108005.
- Um, H. D., *et al*. (2021). Flexible crystalline-silicon photovoltaics: Light management and mechanical design. *Accounts of Materials Research, 2*, 1045-1057.
- van der Burgt, J. S., Verschuuren, M. A., & Polman, A. (2020). Nanophotonic emission control for improved photovoltaic performance. *ACS Photonics, 7*, 2303–2319.
- Varlamov, P., *et al*. (2024). Femtosecond laser ablation and delamination of thin films: Mechanisms and applications. Micromachines, 15(2), 345.
- Veith-Wolf, B. A., *et al*. (2018). Crystalline silicon surface passivation using aluminum oxide. Journal of Applied Physics, 123, 114902.
- Veith-Wolf, B., Hollemann, C., Schulte-Huxel, H., Schmidt, J., & Kessels, W. M. M. (2018). Aluminum oxide for surface passivation and as optical spacer in crystalline silicon solar cells. Solar Energy Materials and Solar Cells, 184, 22–29.
- Wang, F., *et al*. (2021). Full-scale chemical and field-effect passivation: 21.52% efficiency of stable $MAPbI_3$ solar cells via benzenamine modification. Nano Research, 14, 2783–2789.
- Wang, H., Wang, W., & Yu, Z. (2021). Progress in perovskite solar cells towards commercialization: Materials, stability, and modules. Nanomaterials, 11, 861.
- Wang, Y., Zhao, Y., Huang, Q., Su, X., Zhou, J., & Hou, G. (2023). Dopant-free passivating contacts for crystalline silicon solar cells: Progress and prospects. EcoMat, 5(4), e12292.
- Wei, H., Liao, M., Zhao, Y., & colleagues. (2023). Unraveling the passivation mechanisms of c-Si/$SiO_x$/poly-Si contacts. Solar Energy Materials and Solar Cells, 246, 111917.
- Wu, B., & colleagues. (2021). Photon-recycling effect in perovskites for photovoltaic applications. *Optics Letters*.
- Wu, L., *et al*. (2025). Iron-only metasurface broadband absorber for solar energy applications. Nanomaterials, 15(16), 1263.
- Yan, D., Cuevas, A., Michel, J. I., Zhang, C., Wan, Y., Zhang, X., & Bullock, J. (2021). Polysilicon passivated junctions: The next technology for silicon solar cells? Joule, 5(4), 811–828.
- Yang, J., Qu, G., Qiao, Y., Xu, H., Wang, J., Liu, Y., Liu, H., Li, M., Lu, X., Zhang, Z., & Sun, X. (2025). Flexibility meets rigidity: A self-assembled monolayer materials strategy for perovskite solar cells. Nature Communications, 16, 6968.
- Yang, Z., Surrente, A., Galkowski, K., Lai, M. L., Lusakowska, E., Szewczyk, A., … Plochocka, P. (2017). Unraveling the exciton binding energy and the dielectric constant in single crystal methylammonium lead triiodide perovskite. The Journal of Physical Chemistry Letters, 8, 1851–1856.
- Ye, J., *et al*. (2021). Defect passivation in lead-halide perovskite nanocrystals. Angewandte Chemie International Edition, 60(37), 20004–20027.
- Yee, K. S. (1966). Numerical solution of initial boundary value problems involving Maxwell's equations in isotropic media. *IEEE Transactions on Antennas and Propagation, 14*(3), 302–307. Yeh, P. (1988). *Optical waves in layered media*. Wiley.
- Yen, P. (2016). Correlative elemental and electrical micro-analysis of laser fired contacts for silicon solar cells (Master's thesis, MIT).
- Yu, C., Yang, D., Chen, X., & Que, D. (2018). Recent advances in crystalline silicon solar cells. *Crystals, 8*, 430.
- Yu, Z., Raman, A., & Fan, S. (2010). Fundamental limit of nanophotonic light trapping in solar cells. Proceedings of the National Academy of Sciences, 107(41), 17491–17496.
- Yu, Z., Raman, A., & Fan, S. (2011). Nanophotonic light-trapping theory for solar cells. Applied Physics A, 105(2), 329–339.
- Yuan, Y., Li, H., Luo, H., Zhang, Y., Li, X., Jiang, T., Yang, Y., Liu, L., Fan, B., & Hao, X. (2025). A comprehensive review of self-assembled monolayers as hole-transport layers in inverted perovskite solar cells. Energies, 18(10), 2577.
- Zahid, T., Shakeel, R., Rehman, H. M. A., Rafique, S., Ali, T., Parvaiz, M., Kashif, M., Anjum, S., Shah, S. M. W., & Khan, W. Z. (2025). Brain-targeted delivery and redox-responsive release of protein therapeutics via GSH-sensitive $SiO_2$ nanoparticles. Annual Methodological Archive Research Review, 3(7), 648–675. https://doi.org/10.63075/j1p31406
- Zeder, S. G., *et al*. (2022). Assessment of photon recycling in perovskite solar cells. Advanced Energy Materials, 12(17), 2103564.
- Zeng, L., Cai, L., Wang, Z., Chen, N., Liu, Z., Chen, T., Pang, Y., Wang, W., Zhang, H., Zhang, Q., & Gao, P. (2022). High-quality dopant-free electron-selective passivating contact made from ultra-dilute aqueous solution. Nanomaterials, 12(23), 4318.

- Zhang, Y., *et al*. (2022). $PO_x/Al_2O_3$ stacks for c-Si surface passivation. ACS Applied Electronic Materials, 4, 2016–2026.
- Zhou, J., Su, X., Huang, Q., Zhang, B., Yang, J., Zhao, Y., & Hou, G. (2022). Poly-Si/$SiO_x$ passivating contacts for high-efficiency silicon solar cells: Recent advancements and perspectives. Journal of Materials Chemistry A, 10, 20147–20176.
- Zikulnig, J., *et al*. (2022). Photoluminescence imaging for the in-line quality control of CIGS modules. Solar, 2,
- Zuo, S., *et al*. (2025). Picosecond laser processing of ITO and AZO thin films for P1 scribing. Optics Express, 33(21), 43599–43612.